Yang-Lee Quantum Criticality in Various Dimensions

Erick Arguello Cruz,[1] Igor R. Klebanov,[2,3] Grigory Tarnopolsky,[1] and Yuan Xin[1]

[1]*Department of Physics, Carnegie Mellon University, Pittsburgh, Pennsylvania 15213, USA*
[2]*Joseph Henry Laboratories, Princeton University, Princeton, New Jersey 08544, USA*
[3]*Princeton Center for Theoretical Science, Princeton University, Princeton, New Jersey 08544, USA*

(Received 4 June 2025; accepted 3 December 2025; published 9 February 2026)

The Yang-Lee universality class arises when an imaginary magnetic field is tuned to its critical value in the paramagnetic phase of the $d < 6$ Ising model. In $d = 2$, this nonunitary conformal field theory (CFT) is exactly solvable via the $M(2,5)$ minimal model. As found long ago by von Gehlen using exact diagonalization, the corresponding real-time, quantum critical behavior arises in the periodic Ising spin chain when the imaginary longitudinal magnetic field is tuned to its critical value from below. Even though the Hamiltonian is not Hermitian, the energy levels are real due to the $\mathcal{PT}$ symmetry. In this paper, we explore the analogous quantum critical behavior in higher-dimensional non-Hermitian Hamiltonians on regularized spheres S^{d-1}. For $d = 3$, we use the recently invented, powerful fuzzy sphere method, as well as discretization by the platonic solids cube, icosahedron, and dodecahedron. The low-lying energy levels and structure constants we find are in agreement with expectations from the conformal symmetry. The energy levels are in good quantitative agreement with the high-temperature expansions and with Padé extrapolations of the $6-\epsilon$ expansions in Fisher's $i\phi^3$ Euclidean field theory for the Yang-Lee criticality. In the course of this work, we clarify some aspects of matching between operators in this field theory and quasiprimary fields in the $M(2,5)$ minimal model. For $d = 4$, we obtain new results by replacing S^3 with the self-dual polytope called the 24-cell.

DOI: 10.1103/w4qg-2xwn

Subject Areas: Condensed Matter Physics, Particles and Fields, Statistical Physics

I. INTRODUCTION

The Ising model is the most fundamental and widely explored statistical model; it has a broad range of applications. Its one-dimensional version was solved by Ising in 1925 and shown not to possess a finite-temperature phase transition [1]. In all dimensions $d > 1$, however, this model has a line of first-order transitions $T < T_c$, which terminates at the critical point where the $\mathbb{Z}_2$ symmetry is restored. The properties of this second-order phase transition have been studied using many different methods—analytical and numerical. For $d > 4$, the critical exponents of the Ising model are given exactly by Landau's mean field theory, but for $d < 4$, this is no longer the case. Determining the dimension dependence of the critical exponents is a fascinating problem, which continues to attract much attention.

In $d = 2$, the exact Ising critical exponents have been known for many years thanks to the Onsager solution [2]. The critical 2D Ising model corresponds to the simplest unitary Belavin-Polyakov-Zamolodchikov (BPZ) conformal minimal model $M(3,4)$ [3]. More generally, the critical d-dimensional Ising model is described by the continuum theory of a massless scalar field ϕ with an interaction term around ϕ^4. The problem of finding the critical exponents is then mapped to the calculation of the scaling dimensions of operators ϕ, ϕ^2, ϕ^4, etc. In dimensions slightly below 4, the IR fixed point is weakly coupled, and the Wilson-Fisher $4-\epsilon$ expansion [4] provides a useful method for approximating the d dependence of operator dimensions. This case has led to estimates of the 3D Ising critical exponents that are in very good agreement with experiments and Monte Carlo simulations. A significant improvement in accuracy was provided by the numerical conformal bootstrap [5,6], which is based on the conformal symmetry of critical fluctuations [7] (for reviews, see Refs. [8–11]). Furthermore, the numerical bootstrap method has been applied to the operator scaling dimensions in the entire range $2 \leq d < 4$ [12,13], producing excellent agreement with resummed $4-\epsilon$ expansions for the ϕ^4 theory.

More recently, new methods for studying the 3D critical phenomena have emerged [14–18]. They rely on the critical behavior of the quantum theory in $2+1$ dimensions, which is analogous to the well-known periodic quantum spin chains in $1+1$ dimensions. In the continuum limit, the latter give the energy levels on a circle that, via the 2D conformal field theory state-operator map, determine the scaling dimensions of the primary operators and their descendants. To study a 3D CFT in a similar way, one must define the quantum Hamiltonian system on an appropriately regularized sphere S^2. In an important development [14,15,19], the fuzzy sphere regularization [20,21] was shown to work very nicely for the critical 3D Ising model, giving the low-energy states that organize into the expected conformal multiplets (in fact, replacing the S^2 by an icosahedron works quite well, too [17], even though this method does not readily allow for extrapolation to the continuum limit). The fuzzy sphere measurements of various CFT data approximately satisfy the conformal symmetry, which provides nontrivial checks and can also be used to correct the finite-size errors in this approach [18]. The conformal symmetry generators can be directly constructed from the fuzzy sphere observables [22,23]. The fuzzy sphere approach has also been used to study various other 3D CFTs and defect CFTs [24–30].

Besides the scaling dimensions and OPE coefficients in a 3D CFT, the fuzzy sphere approach provides access to the sphere free energy F, which characterizes the number of degrees of freedom [31–33]. This quantity can be extracted from the entanglement entropy across the equator of S^2, and the numerical result for F in the Ising model [16] is in excellent agreement with the extrapolation of the $4-\epsilon$ expansion of F [34].

A fascinating feature of the d-dimensional Ising model is the appearance of zeros of the partition function Z at imaginary values of the magnetic field [35,36]. In the paramagnetic phase $T > T_c$, these Yang-Lee (YL) zeros become dense near the edge value $h_{\rm crit}(T)$. As shown by Kortman and Griffiths [37], the density of zeros has the scaling form $\rho(h) \sim (h - h_{\rm crit}(T))^{\sigma}$, and σ is negative in $d=2$ but positive in $d=3$. In an important further development, Fisher [38] realized that this critical behavior is described by the Euclidean field theory with an imaginary potential proportional to $i\phi^3$. In this continuum approach, the critical exponent is $\sigma = [\Delta_\phi/(d-\Delta_\phi)]$, where Δ_ϕ is the scaling dimension of the real scalar field ϕ. The field theory description of the YL universality class implies that its upper critical dimension is 6. The lower critical dimension is 1, and the exact solution there gives $\sigma = -\frac{1}{2}$ [35,36]. Therefore, an interesting problem is to determine the d dependence of the critical exponents in the range $1 < d < 6$. One approach, analogous to the Wilson-Fisher $4-\epsilon$ expansion for the Ising universality class, is to develop the $6-\epsilon$ expansion for the massless $i\phi^3$ field theory. This approach, in conjunction with the exact result in $d=1$, was used by Fisher [38] to estimate the d dependence of σ for the YL universality class. Soon after the advent of the BPZ minimal models [3], Cardy [39] realized that the critical YL model is also exactly solvable in $d=2$, where it corresponds to the simplest nonunitary minimal model $M(2,5)$ (for a recent review, see Ref. [40]). The field ϕ corresponds to the Virasoro primary $\Phi_{1,2}$ of holomorphic dimension $h_{1,2} = -\frac{1}{5}$. Thus, $\Delta_\phi = -\frac{2}{5}$ and $\sigma = -\frac{1}{6}$ in $d=2$.

In the range $2 < d < 6$, no similar exact results are known. In this paper, we use a combination of $6-\epsilon$ expansions and numerical diagonalizations to approximately determine the scaling dimensions of various operators. The $6-\epsilon$ expansions are available to $O(\epsilon^5)$ [41–43]. Their resummations have been extrapolated to $d=2$, yielding good agreement with $M(2,5)$. However, for the higher-dimension operators, this method can exhibit significant uncertainties. The numerical bootstrap approach is complicated by the fact that the YL model is nonunitary, so the standard methods based on positivity cannot be used. A different bootstrap approach to the YL model was used in Refs. [45–47], but it does not appear to be as precise as the numerical bootstrap based on positivity. We instead follow the successes of the fuzzy sphere [14] and the icosahedron [17,48] approaches to the 3D Ising model, adapting them to the YL case where a non-Hermitian Hamiltonian has to be tuned to quantum criticality. We proceed analogously to the quantum spin chain approach, which has proven to be successful for describing the 2D YL model. Here, an imaginary longitudinal magnetic field h_z was introduced and tuned to a critical value from below [51–54]. Even though the spin chain Hamiltonian is complex, the energy levels are real for $h_z < h_z^{\rm crit}$ due to the $\mathcal{PT}$ symmetry [53].

This paper is organized as follows. In Sec. II, we review the minimal model $M(2,5)$ and its field theory description, discussing the correspondence between the two. In Sec. III, we review the quantum spin chain with an imaginary longitudinal magnetic field [51–53,58]. We carry out its numerical diagonalizations and show that the appropriate criteria for quantum criticality, analogous to those used recently [59] for a precise study of the Ising transition in the Schwinger model, lead to excellent agreement with the exact results from the $M(2,5)$ minimal model. In Sec. IV, we study a quantum spin model with an imaginary longitudinal magnetic field, putting it on the platonic solids cube, icosahedron, and dodecahedron, which are viewed as regularized versions of S^2. We obtain good agreement with the expected YL criticality. In Sec. V, we carry out analogous calculations on the fuzzy sphere and extrapolate them to the thermodynamic limit. Our fuzzy sphere result for the scaling dimension of ϕ, $\Delta_\phi = 0.214(2)$ is in excellent agreement with the high-temperature expansion result 0.214(6) from Ref. [60] and is also very close to our two-sided Padé estimate of approximately 0.218. In Sec. VI, we obtain first results for the quantum criticality of the $d=4$ YL model by replacing S^3 by the 24-cell, which is a self-dual regular 4-polytope.

II. MINIMAL MODEL $M(2,5)$ AND ITS FIELD THEORY DESCRIPTION

The minimal conformal model $M(2,5)$, which describes the YL critical behavior in two dimensions [39], has only one nontrivial Virasoro primary field, $\Phi_{1,2} \equiv \Phi_{1,3}$. It has holomorphic dimension $h_{1,2} = -\frac{1}{5}$. The Kac table of this model, where we denote this field by ϕ, is shown in Table I.

The operator product expansion (OPE) reads

$$\phi(z,\bar{z}) \times \phi(0,0) = |z|^{4/5}\mathrm{I} + C_{\phi\phi\phi}|z|^{2/5}\phi. \quad (2.1)$$

The structure constant is purely imaginary and has the value

$$C_{\phi\phi\phi} = i\left(\frac{\Gamma(\frac{6}{5})^2\Gamma(\frac{1}{5})\Gamma(\frac{2}{5})}{\Gamma(\frac{3}{5})\Gamma(\frac{4}{5})^3}\right)^{1/2} \approx 1.911312699i. \quad (2.2)$$

The lowest-level null vectors in the $M(2,5)$ model are [61,62]

$$L_{-1}|\mathrm{I}\rangle, \qquad \left(L_{-2}^2 + \frac{3}{5}L_{-4}\right)|\mathrm{I}\rangle, \qquad \left(L_{-2} - \frac{5}{2}L_{-1}^2\right)|\phi\rangle,$$
$$\left(L_{-3} - \frac{10}{3}L_{-1}L_{-2} + \frac{25}{36}L_{-1}^3\right)|\phi\rangle. \quad (2.3)$$

All the operators (primary and descendants) up to level 4 are exhibited in Fig. 1, where $T = L_{-2}|\mathrm{I}\rangle$ is the holomorphic part of the stress-energy tensor and

$$Q\phi = \left(L_{-4} - \frac{625}{624}L_{-1}^4\right)|\phi\rangle,$$
$$\bar{Q}\phi = \left(\bar{L}_{-4} - \frac{625}{624}\bar{L}_{-1}^4\right)|\phi\rangle \quad (2.4)$$

denote the spin-4 quasiprimary state [61]. A related spin-0 quasiprimary is $\Xi = Q\bar{Q}|\phi\rangle$ [62].

Using the operator $Q_6 = L_{-6} - \frac{35}{43}L_{-5}L_{-1} - \frac{105}{43}L_{-4}L_{-2}$, we can also construct a spin-6 quasiprimary state [63,64]:

$$Q_6|\phi\rangle, \qquad \bar{Q}_6|\phi\rangle. \quad (2.5)$$

The simplest nonconserved spin-2 quasiprimary is [62]

$$T' = Q_6\bar{Q}|\phi\rangle, \qquad \bar{T}' = Q\bar{Q}_6|\phi\rangle. \quad (2.6)$$

It has dimension $\Delta_{T'} = 9.6$ and lies on the first subleading Regge trajectory.

TABLE I. The $M(2,5)$ model with the central charge $c = -22/5$.

$\Phi_{1,1}$	$\Phi_{1,2}$	$\Phi_{1,3}$	$\Phi_{1,4}$
I	ϕ	ϕ	I

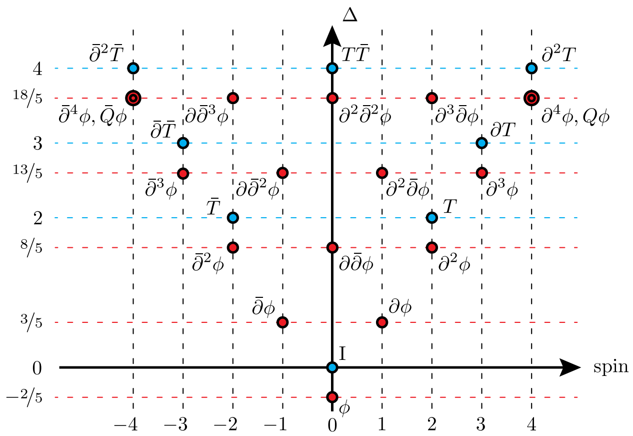

FIG. 1. Lowest dimension operators of $M(2,5)$.

The field theory description of the YL universality class is provided by

$$S = \int d^dx\left(\frac{1}{2}(\partial_\mu\phi)^2 + \frac{g}{6}\phi^3\right), \quad (2.7)$$

where g is purely imaginary [38]. This action has a so-called $\mathcal{PT}$ symmetry [65], which acts by $\phi \to -\phi$, $i \to -i$. In $d = 6 - \epsilon$, the beta function is known to five-loop order [41], but for brevity, we state the results up to three loops [41,66–68]:

$$\beta(g) = -\frac{\epsilon g}{2} - \frac{3g^3}{4(4\pi)^3} - \frac{125g^5}{144(4\pi)^6} - \left(\frac{33085}{20736} + \frac{5\zeta(3)}{8}\right) \times \frac{g^7}{(4\pi)^9} + O(g^9). \quad (2.8)$$

Therefore, there is an IR stable fixed point at

$$g_* = i\sqrt{\frac{2(4\pi)^3\epsilon}{3}}\left(1 + \frac{125}{324}\epsilon + \frac{5(253 - 972\zeta(3))}{26244}\epsilon^2 + O(\epsilon^3)\right). \quad (2.9)$$

In $d = 2$, the field ϕ is identified with the Virasoro primary operator $\Phi_{1,2}$ of the $M(2,5)$ model. The $6 - \epsilon$ expansion of Δ_ϕ is [41,66–68]

$$\Delta_\phi = 2 - \frac{\epsilon}{2} + \gamma_\phi = 2 - \frac{5}{9}\epsilon - \frac{43}{1458}\epsilon^2 + \left(-\frac{8375}{472392} + \frac{8\zeta(3)}{243}\right)\epsilon^3 + O(\epsilon^4). \quad (2.10)$$

Performing Padé extrapolations of this series, which is known to order $O(\epsilon^5)$ [41], with the condition that $\Delta_\phi = -\frac{2}{5}$ in $d = 2$, gives the estimates of its scaling dimension

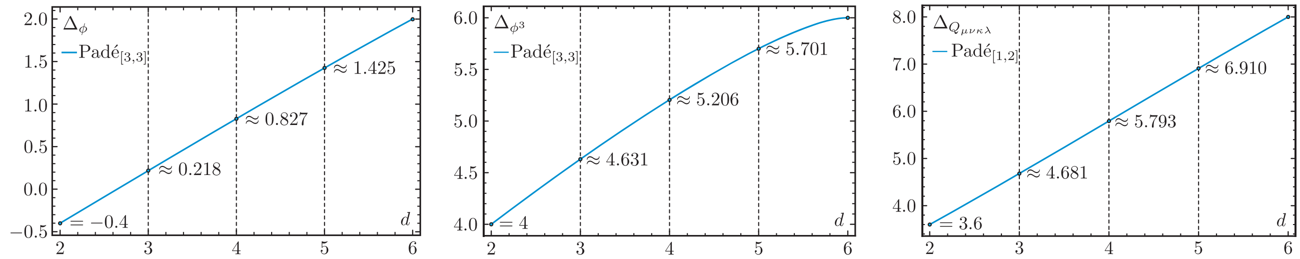

FIG. 2. Two-sided Padé extrapolations of the scaling dimensions of ϕ, ϕ^3 and $Q_{\mu\nu\kappa\lambda}$ operators.

plotted in Fig. 2. The (3, 3) and (4, 2) Padé approximants produce results that are almost indistinguishable. The dependence of Δ_ϕ on d is very smooth and close to linear; see also Table II.

The operator ϕ^2 is a descendant because of the equation of motion. Therefore, the next spin-zero conformal primary field is ϕ^3. Its scaling dimension is [41,66–68]

$$\begin{aligned}\Delta_{\phi^3} &= d + \beta'(g_*) \\ &= 6 - \frac{125}{162}\epsilon^2 + \left(\frac{36755}{52488} + \frac{20\zeta(3)}{27}\right)\epsilon^3 + O(\epsilon^4). \end{aligned} \quad (2.11)$$

Padé extrapolations of this series, which is known to order $O(\epsilon^5)$ [41], indicate that this operator is irrelevant for $d < 6$. In $d = 2$, we identify the $\mathcal{PT}$ invariant operator $i\phi^3$ with the leading $s = 0$ quasiprimary irrelevant operator $T\bar{T}$ of scaling dimension 4. This operator is analogous to the well-known identification of the irrelevant operator ϕ^4 at the IR fixed point of the massless ϕ^4 theory with the operator $T\bar{T}$ in the 2D critical Ising model. Performing Padé extrapolations with the condition that $\Delta_{\phi^3} = 4$ in $d = 2$ gives the estimates of its scaling dimension that are plotted in Fig. 2 and listed for integer d in Table II.

The next spin-zero quasiprimary operator in $M(2,5)$ is $\Xi = Q\bar{Q}\phi$ [62]; it has a rather high scaling dimension, $\frac{38}{5}$. In Ref. [46], this operator was identified with ϕ^3 in the field theory, but our Padé extrapolations of Δ_{ϕ^3} to $d = 2$ are clearly inconsistent with this. We instead propose to identify $Q\bar{Q}\phi$ with field theory operator $i\phi^4$ [69]. Its one-loop scaling dimension can be extracted from the results in Ref. [70], and we find

$$\Delta_{\phi^4} = 8 + \frac{10}{9}\epsilon + O(\epsilon^2). \quad (2.12)$$

Since in $d = 2$ it equals 7.6, its dimension dependence cannot be monotonic, which makes the extrapolation challenging, and we need at least the next term in the series to make quantitative estimates in $d = 3$, 4, 5. We leave this challenge for future work.

The field theory also contains primary operators with an even number of derivatives, which have the schematic form $\phi\partial_{\mu_1}\partial_{\mu_2}\ldots\partial_{\mu_{2n}}\phi + \cdots$. Projecting onto the traceless part of such an operator, we find the leading twist operators of spin $2n$ (they form the leading Regge trajectory). For $n = 1$, this operator is the conserved stress-energy tensor, but for $n > 1$, they are not conserved. The first such operator is the traceless rank-4 tensor

$$Q_{\mu\nu\kappa\lambda} = \phi\partial_\mu\partial_\nu\partial_\kappa\partial_\lambda\phi + \ldots \quad (2.13)$$

In $d = 2$, we identify this operator with the spin-4 quasiprimaries $iQ\phi$ and $i\bar{Q}\phi$ of $M(2,5)$, which have scaling dimension $\frac{18}{5}$. The $6 - \epsilon$ expansion of the dimension of $Q_{\mu\nu\kappa\lambda}$ is [71–74]

$$\Delta_Q = 8 - \frac{16}{15}\epsilon - \frac{871}{30375}\epsilon^2 + O(\epsilon^3). \quad (2.14)$$

Together with the condition that $\Delta_Q = \frac{18}{5}$ in $d = 2$, we find the two-sided Padé estimates shown in Fig. 2 and Table II. The higher spin operators on the leading Regge trajectory can be studied similarly.

The CFT also contains operators of subleading twist. For example, the spin-s operators on the first subleading Regge trajectory have the schematic form $\phi\partial_{\mu_1}\partial_{\mu_2}\ldots\partial_{\mu_s}\partial^2\phi + \cdots$. For $s = 2$, this operator is

TABLE II. Two-sided Padé approximations of the scaling dimensions of the lowest primary operators in $d = 3$, 4, 5. All of them are below the unitarity bounds.

		Two-sided Padé for Δ			
Operators $d=2$	Exact Δ $d=2$	$d=3$	$d=4$	$d=5$	GL description
ϕ	$-2/5$	$0.218_{[3,3]}, 0.218_{[4,2]}$	$0.827_{[3,3]}, 0.827_{[4,2]}$	$1.425_{[3,3]}, 1.425_{[4,2]}$	ϕ
$T\bar{T}$	4	$4.631_{[3,3]}, 4.639_{[4,2]}$	$5.206_{[3,3]}, 5.212_{[4,2]}$	$5.701_{[3,3]}, 5.702_{[4,2]}$	$i\phi^3$
$iQ\phi, i\bar{Q}\phi$	$18/5$	$4.681_{[1,2]}, 4.709_{[2,1]}$	$5.793_{[1,2]}, 5.815_{[2,1]}$	$6.910_{[1,2]}, 6.916_{[2,1]}$	$Q_{\mu\nu\kappa\lambda}$

$$T'_{\mu\nu} = \phi\partial_\mu\partial_\nu\partial^2\phi + \ldots \tag{2.15}$$

Its scaling dimension $\Delta_{T'}(\epsilon) = 8 + O(\epsilon)$ in $d = 6 - \epsilon$. This operator likely extrapolates to the 2D operator (2.6), so $\Delta_{T'}(4) = 9.6$. It would be interesting to study this function, and we leave this for future work [75].

Our Padé extrapolations can be compared with the bootstrap results of Refs. [45–47] and the high-temperature expansions [60]. Some of these results are in good agreement with the estimates in this section. For example, in $d = 3$, the estimate $\Delta_\phi^{\rm boot} \approx 0.213$ from the original paper [45] is close to our value $\Delta_\phi \approx 0.218$ and to the high-temperature expansion result 0.214(6). However, in the later papers [46,47], the bootstrap estimates of Δ_ϕ were revised to 0.235 and 0.174, respectively. These different estimates point to the significant uncertainties in the bootstrap procedure, which are related to the truncation [8]. In addition, some results for the higher operators are further apart. In Ref. [46], the estimate of Δ_{ϕ^3} is approximately 5.0 in $d = 3$ vs our estimate of approximately 4.63. In $d = 4$, Ref. [46] obtained approximately 6.8 vs our finding of approximately 5.2. We find better agreement with the Padé extrapolations from our numerical results on the regularized S^2 and S^3.

III. SPIN CHAIN FOR 2D YANG-LEE MODEL

The Hamiltonian of the 2D Yang-Lee quantum model on a chain with N sites and periodic boundary conditions (PBC) is [51,52,58]

$$H_{\rm YL} = -J\sum_{j=1}^{N} Z_j Z_{j+1} - h_x\sum_{j=1}^{N} X_j - ih_z\sum_{j=1}^{N} Z_j, \tag{3.1}$$

where X and Z are the Pauli matrices and we assume that $Z_{N+1} \equiv Z_1$. The Hamiltonian has $\mathcal{PT}$ symmetry generated by the operator [53]

$$\mathcal{PT} = \prod_{j=1}^{N} X_j \mathcal{T}, \tag{3.2}$$

where $\mathcal{T}$ is complex conjugation. The $\mathcal{PT}$ symmetry acts by $Z_j \to -Z_j$, $i \to -i$.

TABLE III. The $M(3,4)$ model with the central charge $c = 1/2$.

$\Phi_{2,1}$	$\Phi_{2,2}$	$\Phi_{2,3}$
$\Phi_{1,1}$	$\Phi_{1,2}$	$\Phi_{1,3}$
ε	σ	I
I	σ	ε

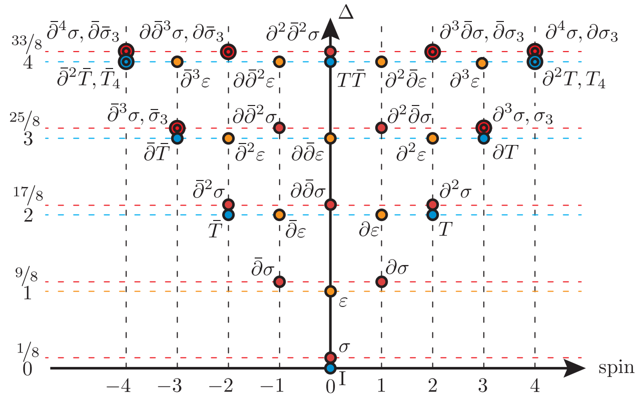

FIG. 3. Lowest dimension operators of $M(3,4)$.

We set $J = 1$ and assume that the system is in the paramagnetic (disordered) phase, so the transverse magnetic field $h_x > h_x^{\rm crit}$, where $h_x^{\rm crit}/J = 1$ is the critical value for the 2D Ising quantum model. It corresponds to the $M(3,4)$ model, whose Kac table is shown in Table III, and all the operators (primary and descendants) up to level $4\frac{1}{8}$ are exhibited in Fig. 3.

The Yang-Lee critical point is reached by tuning the imaginary magnetic field ih_z to the critical point $ih_z^{\rm crit}$. At this critical point, some pairs of energy levels merge, and beyond it, they become complex conjugates of each other.

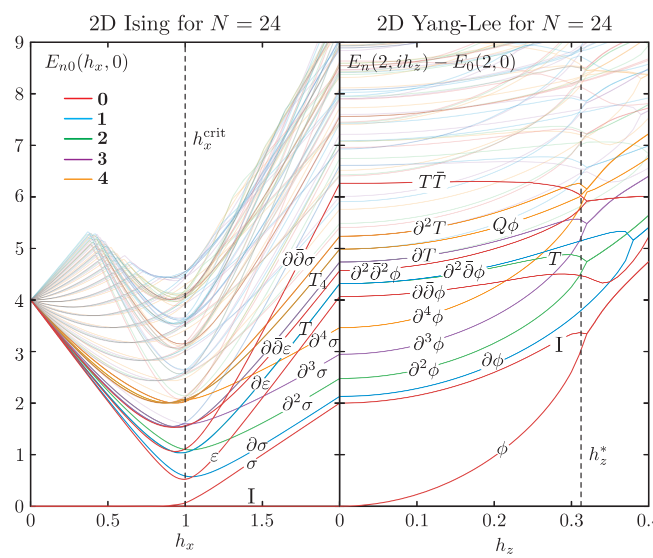

FIG. 4. Energy levels of the Hamiltonian (3.1) for $N = 24$ along the path $(h_x, ih_z) = (0,0) \to (2,0) \to (2, i0.4)$, with $J = 1$. Beyond a merger point, two energy levels become complex conjugate, and we plot their real part (sometimes another transition is visible where the two energies become real again). We identify the lower energy levels with their corresponding operators in the 2D Ising and Yang-Lee CFTs. The first dashed line is the critical point $h_x^{\rm crit} = 1$ for the 2D Ising model, and the second dashed line is the pseudocritical point ih_z^* for the 2D Yang-Lee model, obtained by fixing $r_T = 2$.

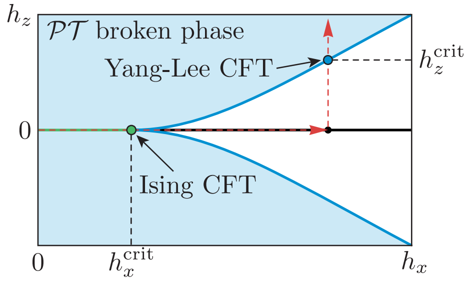

FIG. 5. Qualitative phase diagram of the quantum Ising model with transverse magnetic field h_x and imaginary longitudinal magnetic field h_z. The $h_z = 0$ horizontal line is the $\mathbb{Z}_2$ symmetric line. The Ising critical point, which is located at this line, is shown by the green dot. To the right of this point, the Ising model is in the paramagnetic phase, also known as the high-temperature phase, shown by the black section of the $\mathbb{Z}_2$ symmetric line. The paramagnetic phase with a small h_z deformation still preserves $\mathcal{PT}$ symmetry, shown by the white region. When h_z passes its critical value, the $\mathcal{PT}$ symmetry is spontaneously broken, shown by the blue region. The critical coupling h_z depends on h_x; therefore, we have a line of critical points corresponding to the YL criticality, shown as the blue solid line. We study the Ising-to-YL criticality flow by moving along the red dashed path.

Since the Hamiltonian (3.1) is symmetric, $H_{\rm YL}^T = H_{\rm YL}$, it is pseudo-Hermitian: $H_{\rm YL} = \mathcal{P}H_{\rm YL}^\dagger\mathcal{P}$. In this case, each eigenstate can be assigned an appropriately defined eigenvalue of $\mathcal{PT}$, which is either 1 or -1; it is also known as the Krein signature [76,77]. For $h_z = 0$, the eigenvalue of $\mathcal{PT}$ coincides with the $\mathbb{Z}_2$ eigenvalue of the $\mathcal{P}$ operator. For two states to merge, they must carry opposite eigenvalues of $\mathcal{PT}$ [76–78].

The Hamiltonian (3.1) was studied numerically long ago [51,52,58] and also more recently in Refs. [79,80]. Our numerical results, shown in Fig. 4, are in agreement with these calculations and extend them. For a finite N, mergers of different pairs of levels, which are called "exceptional points" [81], occur at somewhat different values of h_z. However, they are expected to approach the same critical value as $N \to \infty$. The qualitative phase structure in the thermodynamic limit is shown in Fig. 5; we will see that it applies in higher dimensions as well.

TABLE IV. Results for the merging point $ih_z^{\rm merg}$ of the Yang-Lee model on a circular chain for $N = 24$.

h_x	2	3	4	5	10
$h_z^{\rm merg}$	0.314574	0.885528	1.560752	2.294549	6.368703

Figure 4 also shows that, as h_z is increased beyond the merger point, there may be another transition, after which the energy levels become real again. Two energy levels becoming complex conjugates in a small region of parameter space is a common phenomenon in $\mathcal{PT}$-symmetric systems; it occurs due to a small imaginary off-diagonal element in a non-Hermitian Hamiltonian [81]. If the off-diagonal element is very small, the evolution of the two energy levels resembles their crossing. For the pseudo-Hermitian Hamiltonians, such as Eq. (3.1), a pair of energy levels can "cross" only if they have opposite eigenvalues of $\mathcal{PT}$ (Krein signatures) [76–78]. For a Hermitian Hamiltonian, a small off-diagonal element instead produces an avoided crossing of two energy levels.

In search of the YL critical point $ih_z^{\rm crit}$, we may use different criticality criteria that help us define pseudocritical points $ih_z^*(N)$ for given N and h_x, such that when taking the thermodynamic limit of any of them, we must find

$$\lim_{N\to\infty} ih_z^*(N, h_x) = ih_z^{\rm crit}(h_x). \tag{3.3}$$

There are various examples of these criteria: finite-size scaling (FSS) [82–84], extrapolation of merging points [85,86], CFT ratios of energy gaps [59], etc. We define the pseudocritical point as the point at which the following criterion is satisfied:

$$r_T = \frac{E_T - E_{\rm I}}{E_{\partial\phi} - E_\phi} = 2. \tag{3.4}$$

In the numerical spectrum, this ratio can be written using the energy levels of distinct spin sectors, namely, $E_n^{(\mathbf{s})}$ with $n = 0, 1, 2, \ldots$ representing the nth energy level in spin sector $\mathbf{s} = 0, 1, 2, \ldots$, so

$$r_T = \frac{E_1^{(\mathbf{2})} - E_1^{(\mathbf{0})}}{E_0^{(\mathbf{1})} - E_0^{(\mathbf{0})}}. \tag{3.5}$$

TABLE V. Results for the pseudocritical points ih_z^*, defined where $r_T = 2$, and the anomalous dimensions of the operators ϕ, $T\bar{T}$, and $iQ\phi$ for various values of the transverse field h_x, using $N = 24$.

h_x	2	3	4	5	10	Exact
h_z^*	0.312706	0.883574	1.558738	2.292472	6.366335	$\cdots$
Δ_ϕ	−0.375487	−0.3948	−0.400085	−0.402508	−0.406277	−0.4
$\Delta_{T\bar{T}}$	3.615627	3.829043	3.890879	3.919301	3.962861	4
$\Delta_{Q\phi}$	3.612873	3.552427	3.533772	3.524567	3.50883	3.6

Using the values of the pseudocritical points, at fixed N, we can calculate the scaling dimensions of operators using

$$\Delta_{\mathcal{O}} = 2\frac{E_{\mathcal{O}}^{(\mathbf{s})} - E_1^{(\mathbf{0})}}{E_1^{(\mathbf{2})} - E_1^{(\mathbf{0})}}. \tag{3.6}$$

First, in Table IV, we list the position of the merging points of the first two states using $N = 24$ sites.

Using Eq. (3.6), we list the values of the anomalous dimensions for $\mathcal{O} = \phi, T\bar{T}, iQ\phi$ as well as the position of the pseudocritical points, for the case of $N = 24$, in Table V. We see that the pseudocritical points and the merging points are very close to each other.

IV. THE 3D MODEL ON PLATONIC SOLIDS

In this section, we consider the Ising and Yang-Lee models on three 3D platonic solids [17]: the cube, icosahedron, and dodecahedron, which are depicted in Fig. 6. They have, correspondingly, $N = 8$, $N = 12$, and $N = 20$ sites. Apart from these types, there are two other 3D platonic solids: a tetrahedron and an octahedron; they have only $N = 4$ and $N = 6$ sites, so we do not consider them here.

For the schematic Yang-Lee Hamiltonian on the cube, icosahedron, and dodecahedron, we have

$$H_{\mathrm{YL}} = -J\sum_{\langle ij\rangle\in e} Z_i Z_j - h_x\sum_{i\in v} X_i - ih_z\sum_{i\in v} Z_i, \tag{4.1}$$

where the first sum is taken over all the edges of a 3D solid and the last two sums go over the vertices.

These three platonic solids have different ratios of number of vertices N and edges E; therefore, if we want to compare their properties, we have to adjust the couplings J or h_x accordingly. We keep h_x the same for all the platonic solids and adjust only the coupling J. We set $J_{\mathrm{dodecahedron}} = 1$ and adjust other solids' J couplings assuming that $JE/N = \mathrm{const}$. Therefore, we find $J_{\mathrm{cube}} = 1$ and $J_{\mathrm{icosahedron}} = 3/5$. We plot the energy gaps of the Hamiltonian (4.1) for the icosahedron and dodecahedron in Fig. 7. In Table VI, we list values for the merger point ih_z^{merg} of the two lowest states: $|\mathrm{I}\rangle$ and $|\phi\rangle$, which correspond to the lowest energy levels $E_0^{(\mathbf{1})}$ and $E_1^{(\mathbf{1})}$ in

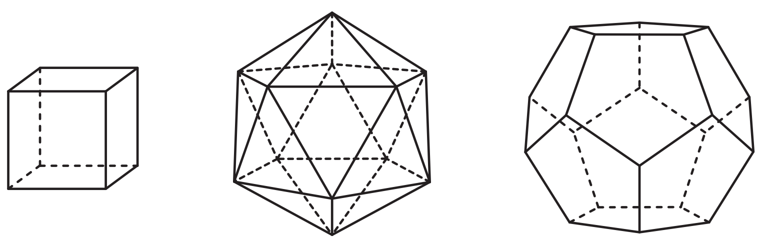

FIG. 6. Three-dimensional platonic solids (N, E): cube (8, 12), icosahedron (12, 30), and dodecahedron (20, 30).

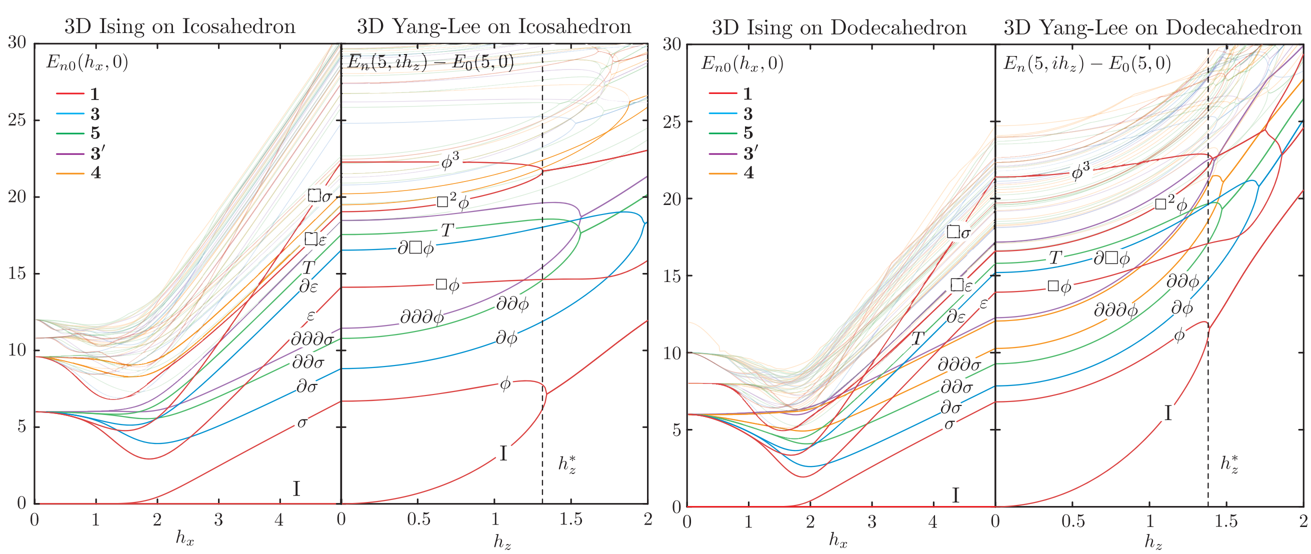

FIG. 7. Energy gaps of the Hamiltonian (4.1) for the icosahedron and dodecahedron along the path $(h_x, ih_z) = (0,0) \to (5,0) \to (5, i2)$, where $J = 3/5$ for the icosahedron and $J = 1$ for the dodecahedron. We identify the lower energy levels with their corresponding operators in the Ising and Yang-Lee CFTs. The dashed line is the pseudocritical point ih_z^* obtained by fixing $r_T = 3$.

TABLE VI. Results for the merger point ih_z^{merg} of the Yang-Lee model on the cube, icosahedron, and dodecahedron.

h_x	5	10	15	20	25	30	35	40	45	50
C: h_z^{merg}	1.513	5.173	9.283	13.591	18.016	22.517	27.074	31.674	36.307	40.968
I: h_z^{merg}	1.339	4.926	8.991	13.265	17.661	22.138	26.673	31.253	35.868	40.513
D: h_z^{merg}	1.387	5.020	9.112	13.406	17.817	22.308	26.855	31.438	36.071	40.723

the singlet representation **1** of 3D symmetry point groups. Below, we use the notation $E_n^{(\mathbf{r})}$ for the energy level n in irrep $\mathbf{r}$ of the point group.

The other criticality criteria for the pseudocritical point ih_z^* corresponds to fixing the ratio

$$r_T \equiv \frac{E_T - E_{\mathrm{I}}}{E_{\partial\phi} - E_\phi} \tag{4.2}$$

to be exactly $r_T = 3$. Numerically, this ratio can be obtained by using the following energy levels in different irreps of O and I:

$$\text{cube:}\ r_T = \frac{E_1^{(\mathbf{3}')} - E_0^{(\mathbf{1})}}{E_0^{(\mathbf{3})} - E_1^{(\mathbf{1})}},$$
$$\text{icosahedron/dodecahedron:}\ r_T = \frac{E_1^{(\mathbf{5})} - E_0^{(\mathbf{1})}}{E_0^{(\mathbf{3})} - E_1^{(\mathbf{1})}}, \tag{4.3}$$

where $\mathbf{5}_{O(3)}$ splits as $\mathbf{2} + \mathbf{3}'$ under the cubic symmetry group O; it does not split for the icosahedral group I, and $\mathbf{1}_{O(3)}$ and $\mathbf{3}_{O(3)}$ do not split for O and I and correspond to irreps **1** and **3**. Here, we list values ih_z^*, where $r_T = 3$ in Table VII. These values are slightly away from the merger points listed in Table VI. We can compute the anomalous dimension Δ_ϕ as

$$\text{cube:}\ \Delta_\phi = 3\frac{E_1^{(\mathbf{1})} - E_0^{(\mathbf{1})}}{E_1^{(\mathbf{3}')} - E_0^{(\mathbf{1})}},$$
$$\text{icosahedron/dodecahedron:}\ \Delta_\phi = 3\frac{E_1^{(\mathbf{1})} - E_0^{(\mathbf{1})}}{E_1^{(\mathbf{5})} - E_0^{(\mathbf{1})}}. \tag{4.4}$$

We list values for Δ_ϕ computed at the pseudocritical point ih_z^*, where $r_T = 3$, in Table VIII.

The results of this section show that the platonic solid regulators of the sphere give a good indication of the YL quantum criticality, in spite of the fact that there are only three possible numbers of lattice sites. However, the determination of scaling dimensions is not as precise as in the fuzzy sphere method that we will use in the next section. In order to improve the platonic solid approach to YL criticality, one can use the conformal perturbation theory, which was shown to work well for the platonic solid approach to the 3D Ising model [17,18]. We leave this for future work.

V. THE 3D MODEL ON FUZZY SPHERE

A. Fuzzy sphere approach to Yang-Lee quantum criticality

In this section, we use the fuzzy sphere regulator for S^2, which is a novel setup using the quantum Hall system. It is analogous to quantum spin systems but preserves the SO(3) symmetry. The model describes nonrelativistic fermions projected to the lowest Landau level (LLL) with quadratic and quartic couplings [14,22],

TABLE VII. Results for the Yang-Lee pseudocritical point ih_z^* defined by the criteria $r_T = 3$.

h_x	5	10	15	20	25	30	35	40	45	50
C: h_z^*	1.467	5.140	9.252	13.560	17.984	22.485	27.042	31.641	36.274	40.934
I: h_z^*	1.312	4.907	8.973	13.247	17.643	22.120	26.655	31.234	35.849	40.493
D: h_z^*	1.381	5.015	9.107	13.41	17.813	22.303	26.850	31.441	36.065	40.718

TABLE VIII. Results for Δ_ϕ at the pseudocritical point ih_z^*, where $r_T = 3$.

h_x	5	10	15	20	25	30	35	40	45	50
C: Δ_ϕ	0.424	0.346	0.323	0.312	0.305	0.300	0.297	0.294	0.292	0.290
I: Δ_ϕ	0.385	0.306	0.283	0.272	0.265	0.260	0.257	0.254	0.252	0.250
D: Δ_ϕ	0.289	0.244	0.233	0.228	0.224	0.222	0.221	0.220	0.219	0.218

$$
\begin{aligned}
H &= H_4 + H_2, \\
H_4 &= R^2 \int d^2\Omega[\lambda_n(\psi^\dagger\psi)U(\psi^\dagger\psi) - \lambda_{n,z}(\psi^\dagger\sigma_z\psi)U(\psi^\dagger\sigma_z\psi)], \\
H_2 &= -R^2 \int d^2\Omega[h_x(\psi^\dagger\sigma_x\psi) + ih_z(\psi^\dagger\sigma_z\psi)],
\end{aligned}
\tag{5.1}
$$

where $U = \sum_n a_n \nabla^{2n}$ is a contact potential that can be written as a series of derivative operators. We follow the same setup as Refs. [14,22] and set $\lambda_n = \lambda_{n,z}$. We can expand the above Hamiltonian using the fermion creation and annihilation operators. The current-current four-body interaction term is [14]

$$
\begin{aligned}
H_4 = \frac{1}{2} \sum_{m_{1,2,3,4}=-s}^{s} & V_{m_1,m_2,m_3,m_4} \delta_{m_1+m_2,m_3+m_4} \\
& \times [(\mathbf{c}^\dagger_{m_1}\mathbf{c}_{m_4})(\mathbf{c}^\dagger_{m_2}\mathbf{c}_{m_3}) - (\mathbf{c}^\dagger_{m_1}\sigma^z\mathbf{c}_{m_4})(\mathbf{c}^\dagger_{m_2}\sigma^z\mathbf{c}_{m_3})],
\end{aligned}
\tag{5.2}
$$

where $\mathbf{c}_{m_1} = \binom{c_{m,\uparrow}}{c_{m,\downarrow}}$. The coefficient tensor

$$
\begin{aligned}
V_{m_1,m_2,m_3,m_4} = \sum_l V_l(4s-2l+1) & \begin{pmatrix} s & s & 2s-l \\ m_1 & m_2 & -m_1-m_2 \end{pmatrix} \\
\times & \begin{pmatrix} s & s & 2s-l \\ m_4 & m_3 & -m_3-m_4 \end{pmatrix}
\end{aligned}
\tag{5.3}
$$

is parametrized by the Haldane pseudopotentials V_l. In our work, we truncate the potential to V_0 and V_1, which is equivalent to the derivative expansion truncated to order ∇^2. The overall normalization is fixed with $V_1 = 1$, and V_0 is a tunable parameter of the model. The LLL-projected Hamiltonian has $(4s+2)$ levels. We fill the total number of $N = 2s+1$ fermions in these levels. Under half-filling, the charge degrees of freedom are gapped, and the particle-hole symmetry is preserved. The total number of spins, N, can be treated as a UV cutoff, which can be most clearly seen from the fact that the commutator $\{\psi(\Omega), \psi(\Omega')\}$ approaches a delta function of size $\sqrt{1/N}$. This approach allows us to identify the radius of the sphere as $R \sim \sqrt{N}$.

The density terms H_2 can be written as

$$
\begin{aligned}
H_2 &= -h_x H_X - ih_z H_Z, \\
H_X &= \sum_{m=-s}^{s} \mathbf{c}^\dagger_m \sigma^x \mathbf{c}_m, \\
H_Z &= \sum_{m=-s}^{s} \mathbf{c}^\dagger_m \sigma^z \mathbf{c}_m.
\end{aligned}
\tag{5.4}
$$

The two-body terms are chosen so that the Hamiltonian mimics the quantum spin model setup in previous sections with the identification

$$
H_{\mathrm{YL}}(V_0, h_x, ih_z) = H_{\mathrm{Ising}}(V_0, h_x) - ih_z H_Z, \tag{5.5}
$$

where the Ising part of the Hamiltonian,

$$
H_{\mathrm{Ising}} = H_4(V_0) - h_x H_X, \tag{5.6}
$$

follows the original setup of Ref. [14]. The fuzzy sphere Ising Hamiltonian is analogous to the lattice quantum Ising model that has a ZZ nearest coupling term and a transverse field X. Apart from the SO(3) symmetry, the Ising Hamiltonian has a spin-flip $\mathbb{Z}_2$ symmetry that takes $\mathbf{c}_m \mapsto \sigma_x \mathbf{c}_m$, but this symmetry is explicitly broken by the H_Z horizontal field term. This term also breaks Hermiticity. The Yang-Lee Hamiltonian is still invariant under a combination of spin-flip and complex conjugation, which serves as the $\mathcal{PT}$ symmetry. The eigenvalues of the $\mathcal{PT}$ symmetric Hamiltonian are real numbers or pairs of conjugate complex numbers. Under half-filling, the system also has a particle-hole symmetry $\mathbf{c}_m \mapsto i\sigma_y \mathbf{c}_m, i \to -i$, which can be interpreted as the spatial parity symmetry in the thermodynamic limit.

We expect the phase diagram of the Hamiltonian (5.5) to be the same as in Fig. 5. Similar to the 2D case, there is a phase transition when we take the Ising model in the paramagnetic phase and turn on an imaginary longitudinal magnetic field h_z. To show the qualitative behavior of the phase transition, it is helpful to identify the correspondence of low-lying eigenstates between Ising criticality and YL criticality. We scan coupling constants h_x and ih_z along the red-dashed trajectory in Fig. 5 and keep track of a number of eigenvalues. The Ising criticality is reported in Ref. [14] to occur at couplings $V_0 = 4.75$ and $h_x = 3.16$. We hold V_0 fixed throughout the trajectory. We gradually increase h_x from 0 to 10 and then increase h_z from 0 to $h_z \approx 5.2$. The spectrum along this trajectory is shown in Fig. 8, where we can identify the tower of operators that belong to the 3D YL universality class.

A summary of the operator flow is presented in Table IX, as are the first, low-lying, merging Yang-Lee states. We note that all flows between these low-lying operators in both CFTs admit a clear interpretation in the GL description. For example, both σ and ϕ correspond to the ϕ field in the ϕ^4 and $i\phi^3$ models. The operator ε corresponds to ϕ^2 in the ϕ^4 model, and ϕ^2 coincides with $\Box\phi$ in the $i\phi^3$ model due to the equations of motion. Likewise, the operator $\Box\sigma$ coincides with ϕ^3 in the ϕ^4 model for the same reason and appears as the ϕ^3 operator in the $i\phi^3$ model. Thus, we conjecture that ε', which corresponds to ϕ^4 in the ϕ^4 model, also represents ϕ^4 in the $i\phi^3$ model. A similar approach applies to the other primary operators and their descendants.

Finally, we notice that operators from different sectors of the Ising-$\mathbb{Z}_2$ symmetry and equal spin on the left ($ih_z = 0$) merge on the Yang-Lee side on the right ($ih_z \neq 0$), where such symmetry is explicitly broken; e.g., I merges with σ

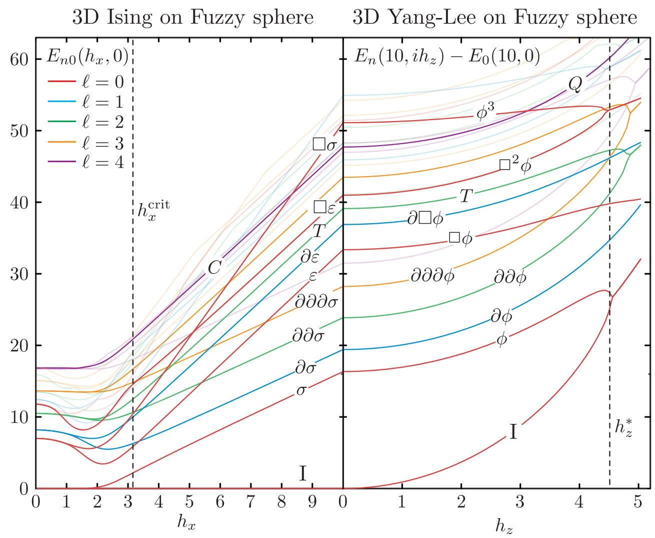

FIG. 8. Energy gaps of the fuzzy sphere Hamiltonian (5.5) along the path $(h_x, ih_z) = (0,0) \to (10,0) \to (10, i5.2)$, where $N = 12$, $V_0 = 4.75$. We identify the lower energy levels with their corresponding operators in the Ising and Yang-Lee CFTs. The dashed lines are the Ising critical point $h_x^{\mathrm{crit}} \approx 3.16$ and the Yang-Lee pseudocritical point $ih_z^* \approx 4.5$ obtained by fixing $r_T = 3$. We notice that operators with the same spin that merge near ih_z^* always come from different $\mathbb{Z}_2$ Ising sectors; hence, they have opposite eigenvalues of $\mathcal{PT}$.

and $\Box\varepsilon$ merges with $\Box\sigma$ at some ih_z value. This finding is consistent with the general result, reviewed in Sec. III, that a pair of levels can merge only if they have opposite eigenvalues of $\mathcal{PT}$.

B. Approaching the 3D YL critical point

Among the list of possibilities to define a pseudocritical point, we follow both the 2D and platonic solids sections and find that one of the most suitable criteria is through the use of the stress tensor, whose scaling dimension at the critical point is $\Delta_{T_{\mu\nu}} = 3$. Therefore, as before, we consider the expression

$$r_T = \frac{E_T(N) - E_{\mathrm{I}}(N)}{E_{\partial\phi}(N) - E_{\phi}(N)} = 3 \tag{5.7}$$

as our criticality criterion. In fuzzy sphere regularization, this corresponds to the ratio of the following levels (same as in the icosahedron case):

$$r_T = \frac{E_1^{(\mathbf{5})} - E_0^{(\mathbf{1})}}{E_0^{(\mathbf{3})} - E_1^{(\mathbf{1})}} = 3. \tag{5.8}$$

The identification of each state is taken from the operator flow from Ising to Yang-Lee, shown in Fig. 8 and Table IX. Note that the expression (5.7) does not depend on the scaling dimension of ϕ, which we will find later. Thus, we obtain $ih_z^*(N)$ for $N = 8, 9, \ldots, 14$, and the IR critical point is extrapolated via Eq. (3.3) using the $1/N$ linear fit [87]. In Fig. 9, we show an example of thermodynamic critical point extrapolation as a function of N for distinct criticality criteria [88]; we can see they all converge to the same value within about 1%, and we notice that ih_z^{crit} is far from its pseudocritical counterpart for small N, in contrast to the 2D case, where ih_z^{crit} and $ih_z^*(N)$ lie within a small perturbative regime [85]. We present some of the extrapolated critical points for various h_x in Table X, and we observe that the deeper we go into the paramagnetic phase ($h_x > 3.16$), the better the convergence; however, if we take a very big h_x,

TABLE IX. Top: summary of the first CFT operators of the 3D Ising model and their corresponding trajectories to the 3D YL ones in each spin sector. The operator $C_{\mu_1\mu_2\mu_3\mu_4}$ is the first $\mathbb{Z}_2$-even, parity-even, spin-4 primary in 3D Ising CFT. Bottom: low-lying spectrum merging states in the 3D Yang-Lee model.

Operator flow from 3D Ising CFT to 3D YL CFT	
Ising ($\ell = 0$)	YL ($\ell = 0$)
I	I
σ	ϕ
ε	$\Box\phi$
$\Box\varepsilon$	$\Box^2\phi$
$\Box\sigma$	ϕ^3
ε'	ϕ^4
Ising ($\ell = 1$)	YL ($\ell = 1$)
$\partial_\mu\sigma$	$\partial_\mu\phi$
$\partial_\mu\varepsilon$	$\partial_\mu\Box\phi$
Ising ($\ell = 2$)	YL ($\ell = 2$)
$\partial_{\mu_1}\partial_{\mu_2}\sigma$	$\partial_{\mu_1}\partial_{\mu_2}\phi$
$T_{\mu\nu}$	$T_{\mu\nu}$
$T'_{\mu\nu}$	$T'_{\mu\nu}$ (2.15)
Ising ($\ell = 3$)	YL ($\ell = 3$)
$\partial_{\mu_1}\partial_{\mu_2}\partial_{\mu_3}\sigma$	$\partial_{\mu_1}\partial_{\mu_2}\partial_{\mu_3}\phi$
$\partial_\alpha T_{\mu\nu}$	$\partial_\alpha T_{\mu\nu}$
Ising ($\ell = 4$)	YL ($\ell = 4$)
$\partial_{\mu_1}\partial_{\mu_2}\partial_{\mu_3}\partial_{\mu_4}\sigma$	$\partial_{\mu_1}\partial_{\mu_2}\partial_{\mu_3}\partial_{\mu_4}\phi$
$\partial_{\alpha_1}\partial_{\alpha_2}T_{\mu\nu}$	$\partial_{\alpha_1}\partial_{\alpha_2}T_{\mu\nu}$
$C_{\mu_1\mu_2\mu_3\mu_4}$	$Q_{\mu_1\mu_2\mu_3\mu_4}$

Merging states in 3D YL	
Merger 1	Merger 2
I	ϕ
$\partial_\mu\phi$	$\partial_\mu\Box\phi$
$\partial_\mu\partial_\nu\phi$	$T_{\mu\nu}$
$\partial_\alpha\partial_\mu\partial_\nu\phi$	$\partial_\alpha T_{\mu\nu}$
$\Box^2\phi$	ϕ^3
$\partial_{\mu_1}\partial_{\mu_2}\partial_{\mu_3}\partial_{\mu_4}\phi$	$\partial_{\mu_1}\partial_{\mu_2}T_{\mu_3\mu_4}$

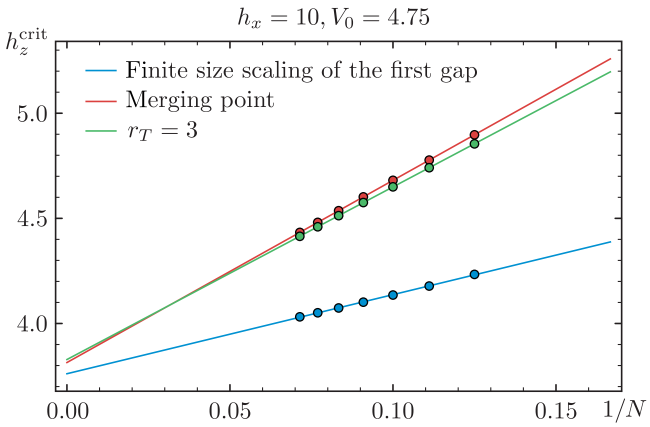

FIG. 9. Yang-Lee thermodynamic critical point h_z^{crit} extrapolation for $h_x = 10$ and $V_0 = 4.75$ with $N \in [8, 14]$ using different criticality criteria. The extrapolation is performed by a linear fit in $1/N$. The results agree within a 10^{-2} error.

then we start facing numerical convergence problems. Therefore, we choose $h_x \in [4, 100]$.

C. Extracting the CFT data

The most remarkable feature of the fuzzy sphere model is that it realizes CFTs in radial quantization, where conformal invariant data such as the scaling dimensions and OPE coefficients can be directly extracted from simple observables in the fuzzy sphere setup. In this subsection, we discuss the extraction of these data numerically. Throughout this subsection, we pick the critical point of the system at fixed $V_0 = 4.75$ and $h_x = 20$, tuning ih_z to the pseudocritical coupling $ih_z^*(N)$. The criterion we use for the pseudocritical point is the CFT ratio of the stress tensor (5.7); in other words, we fix $\Delta_{T^{\mu\nu}} = 3$. The rest of the CFT data will have finite-size deviation from the CFT values, and we study the extrapolation to the thermodynamic limit $N \to \infty$ numerically. We use a publicly available code package (*FuzzifiED*) [89] and compute the eigensystem through exact diagonalization up to $N = 18$. Extrapolation to the thermodynamic limit is performed by fitting the data from $N = 12$ to $N = 18$ as a function of N using models motivated by the finite-size scaling properties of CFTs, also known as conformal perturbation theory [17,18,90,91].

CFT systems have many symmetries. In the fuzzy sphere realization, this implies that any conformally invariant quantity can be extracted in many ways. We see remarkable agreement between many distinct ways to evaluate the same quantity, which provides nontrivial validation of our numerical procedure. In this section, we discuss these approaches in detail.

TABLE X. Results of pseudocritical points h_z^* using $r_T = 3$ for $N = 14$ and thermodynamic critical points using various criticality criteria for distinct values of h_x and fixed $V_0 = 4.75$.

h_x	4	6	8	10	11
h_z^*	0.465609	1.60018	2.9475	4.41454	5.17874
h_z^{crit}	0.20(2)	1.16(3)	2.41(4)	3.80(4)	4.53(4)

In Table XI, we summarize our key numerical results for the CFT data of the 3D YL criticality. Some of the quantities have been computed in the literature [41,46,47,60], and we list them in the table for comparison. The data are from Eqs. (5.15), (5.16), (5.26), (5.31), and (5.39).

1. Scaling dimensions

In radial quantization, the CFT states and local operators have one-to-one correspondence. The CFT Hamiltonian is the dilatation operator; thus, CFT local operators correspond to eigenstates, and the associated eigenvalues are the scaling dimension. Each eigenstate also diagonalizes global symmetry quantum numbers, which are total spin ℓ, spin-z projection ℓ_z, and the spacetime parity p. The ground state always has spin 0.

In the fuzzy sphere realization, the energy levels can be shifted by an arbitrary ground-state energy and rescaled by a model-dependent speed of light. Therefore, we read off the CFT scaling dimensions as ratios. We assume that the lowest spin-0 state, the second-lowest spin-0 state, and the lowest spin-1 state correspond to identity I, the fundamental primary operator ϕ, and its descendant $\partial\phi$ operators, respectively. The difference between the scaling dimensions of the primary and its first descendant is $\Delta_{\partial\phi} - \Delta_\phi = 1$, which provides us with a simple way to rescale the energy eigenvalues to match the CFT scaling dimensions, as in Eq. (5.7). For each state, the scaling dimension of the corresponding local operator is

$$\Delta_{\mathcal{O}} = 3\frac{E_{\mathcal{O}} - E_{\mathrm{I}}}{E_T - E_{\mathrm{I}}}, \tag{5.9}$$

where E_{I} is the ground-state energy. All CFT data extracted from the fuzzy sphere Hamiltonian at finite N will have finite-size errors; therefore, we need to study the finite-size scaling behavior of the CFT data. The finite-size model near criticality is described by a CFT action with relevant and irrelevant deformations [17,18,90,92–94]:

$$S = S_{\mathrm{CFT}} + \frac{g_\phi}{N^{(\Delta_\phi - d)/2}}\int d^d x \phi(x) + \sum_i \frac{g_i}{N^{(\Delta_i - d)/2}}\int d^d x \mathcal{O}_i(x), \tag{5.10}$$

where we separate the relevant deformation ϕ and other operators $\mathcal{O}_i$, which are all irrelevant, and g_ϕ and g_i are dimensionless couplings. Near the criticality, the separation of scales is given by $(\Lambda_{\mathrm{UV}}/\Lambda_{\mathrm{IR}}) \sim \sqrt{N}$, which provides the volume dependence of the couplings. The energy eigenvalues of the finite Hamiltonian match the CFT Hamiltonian as

TABLE XI. CFT data from the fuzzy sphere results. We also list the values from other approaches for comparison. The subscript $[E]$ represents data extracted from eigenvalues. Subscripts $[Z]$ and $[X]$ represent data extracted from the matrix element of the fuzzy sphere Z_ℓ and X_ℓ observables, respectively. Other subscripts represent the Padé level used. The error bars of the fuzzy sphere estimations are drawn from the largest differences of the extrapolations shown in the corresponding plots. They show the scales of possible fitting errors and should not be understood as bounds on the true values.

Observable	Fuzzy sphere	Padé	Two-sided Padé	Five-loop All [41]	Truncated Bootstrap [46]	High-temperature expansion [60]
Δ_ϕ	$0.214(2)_{[E]}$ $0.2155(16)_{[Z]}$ $0.2151(8)_{[X]}$	$0.222_{[3,2]}$	$0.218_{[3,3]}$ $0.218_{[4,2]}$	0.215(10)	0.235(3) 0.174 [47]	0.214(6)
Δ_{ϕ^3}	$4.613(6)_{[E]}$	$4.766_{[3,2]}$	$4.631_{[3,3]}$ $4.639_{[4,2]}$	4.5(2)	5.0(1)	
$\Delta_{Q_{\mu\nu\kappa\lambda}}$	$4.9(1)_{[E]}$	$4.519_{[1,1]}$	$4.681_{[1,2]}$ $4.709_{[2,1]}$		4.75(1)	
$\lvert C_{\phi\phi\phi}\rvert$	$1.9696(31)_{[Z]}$ $1.969(5)_{[X]}$				1.9697(25)	
$\lvert C_{\phi\phi\phi^3}\rvert$	$0.026(7)_{[Z]}$ $0.0238(15)_{[X]}$					
$\lvert C_{\phi^3\phi\phi^3}\rvert$	$1.3774(9)_{[Z]}$ $1.364(7)_{[X]}$					
$\lvert C^{(0)}_{T\phi T}\rvert$	$1.157(2)_{[Z]}$ $1.141(14)_{[X]}$					

$$E_n = E_0 + \frac{\nu}{\sqrt{N}}\left(H_{\mathrm{CFT}} + \frac{g_\phi}{N^{(\Delta_\phi - d)/2}}\int d^{d-1}\Omega\phi(\Omega) + \sum_i \frac{g_i}{N^{(\Delta_i - d)/2}}\int d^{d-1}\Omega\mathcal{O}_i(\Omega)\right), \tag{5.11}$$

where $H_{\mathrm{CFT}}|n\rangle = \Delta_n|n\rangle$, and Δ_n are the CFT scaling dimensions. The relevant (irrelevant) couplings g_ϕ (g_i) contribute to the leading conformal perturbation corrections to these eigenvalues through diagonal matrix elements with a growing (suppressed) volume dependence.

In this work, we measure the spectrum at the pseudocritical point defined when the stress-tensor scaling dimension matches $\Delta_{T_{\mu\nu}} = d = 3$, as described in Eq. (5.7). Thus, the deformation couplings cancel for the specific ratio in Eq. (5.7) to give 3. Using the matching formula (5.11), and expanding Eq. (5.7) to the first order in g, we can determine that

$$g_\phi \propto N^{(\Delta_\phi - \Delta_{\mathcal{O}_I})/2}, \tag{5.12}$$

where $\mathcal{O}_I$ represents the leading irrelevant deformation. Thus, the contribution from the relevant deformation and the leading irrelevant deformation are at the same order of magnitude, assuming the dimensionless coupling constant of the irrelevant deformation g_I is of order 1. From this starting point, we see that the eigenvalues determined using the ratios in Eq. (5.9) will contain a finite-size error as

$$\Delta^{(N)} = \Delta + cN^{(3-\Delta_{\mathcal{O}_I})/2} + \cdots \tag{5.13}$$

where c is some dimensionless coefficient that depends on g_I. The subleading couplings g_i are suppressed, but they also contribute. A comprehensive conformal perturbation analysis will help determine the explicit form of the correction terms and provide a more accurate determination of the spectrum by fitting multiple scaling dimensions using parameters g_I, Δ_I, and the corresponding OPE coefficients, which is beyond the scope of this work. In this work, we try accounting for the finite-size error by fitting a single eigenvalue as a function of N. Our fitting model is

$$\Delta^{(N)} = P_{w,K}(N) \equiv \Delta + \sum_{k=0}^{K} a_k \frac{1}{N^{w+k/2}}, \tag{5.14}$$

where Δ is the scaling dimension prediction extrapolated to the thermodynamic limit. The model is essentially a polynomial in $(1/R) = (1/\sqrt{N})$ except it begins at power w. We choose this model because it takes into account that the leading correction comes in a specific power $N^{(3-\Delta_{\mathcal{O}_I})/2}$ in conformal perturbation theory, and the series expansion after the leading term is agnostic about the precise form of subleading irrelevant deformations and higher-order perturbation theory, which we do not know precisely. For the 3D Yang-Lee criticality, it is likely that the irrelevant deformation $\mathcal{O}_I$ is the subleading scalar primary operator, which has a Ginzburg-Landau description ϕ^3. From $(6-\epsilon)$ expansion

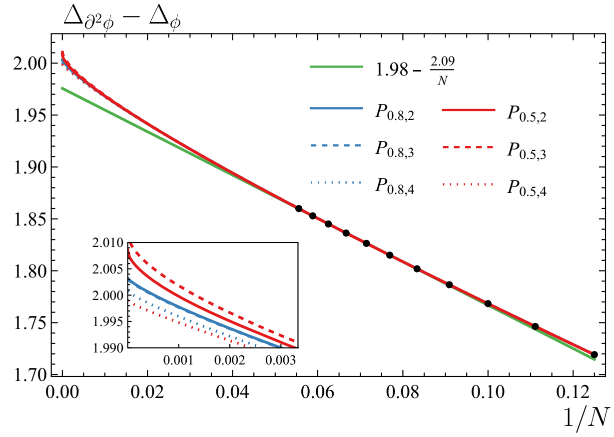

FIG. 10. Testing the fitting scheme (5.14) on a known level difference $\Delta_{\partial^2\phi} - \Delta_\phi = 2$. Conformal perturbation theory suggests that the beginning power should be $w = 0.8$. We also try $w = 0.5$, which amounts to a Taylor series in $1/R$ and a linear fit in $1/N$. For both nonlinear models, we vary the truncation level K from 2 to 4. The result shows that the nonlinear model significantly improves the fit compared to the linear model, and the end result is not sensitive to the parameters.

and from our fuzzy sphere data, we see that $\Delta_{\phi^3} \approx 4.6$, and we set $w = 0.8$. The extrapolations from the fit should not be, and are not, sensitive to the precise value of the input power w. For the number of powers we keep, we use $K = 3$, which works for most energy levels except for a few. We detect that K is too high if the coefficients of the powers abruptly increase. To validate the fitting scheme, we test it on the difference between two levels $\Delta_{\partial^2\phi} - \Delta_\phi$, which we expect to be 2. In Fig. 10, we plot numerical results for $\Delta_{\partial^2\phi} - \Delta_\phi$ together with several different fitting schemes. A linear extrapolation still visibly deviates from 2. A higher power series fit brings us significantly closer to the theoretical value. The precise value of the power does not matter very much, so the extrapolations from various powers w and truncations K agree to the third digit, though $w = 0.8$, the more informed guess from conformal perturbation theory, is more stable against small changes in truncation power.

In Fig. 11, we show the low spectrum of 3D YL criticality as a result of the extrapolation. In the extrapolation scheme (5.14), we treat each eigenvalue independently, so the conformal algebra is not taken as an input except for rescaling the gap between Δ_ϕ and $\Delta_{\partial\phi}$ to 1. In the plot, we see that the relation between Δ_ϕ and the descendant levels is precisely integers, making it easy to distinguish primary from descendant levels. The scaling dimension of the stress tensor is fixed at $\Delta_{T_{\mu\nu}} = 3$ by the criticality criterion, and all its descendants in this plot are integers to a high precision. The plot shows two other primaries, one at $(\ell = 0, \Delta \approx 4.6)$ and the other at $(\ell = 4, \Delta \approx 4.9)$. The former agrees with the $(6 - \epsilon)$ expansion prediction of the ϕ^3 operator in the Ginzburg-Landau description, and the latter seems to belong to the leading double trace family

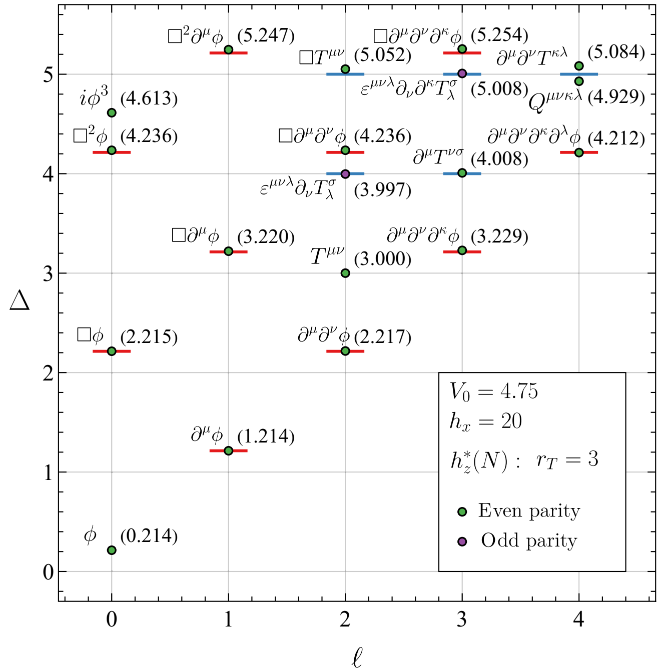

FIG. 11. Estimation of the low-lying spectrum for the critical 3D YL model. We extrapolate the eigenvalues from $N = 12$ to $N = 18$ to the thermodynamic limit using model $P_{0.8,K}$ defined in Eq. (5.14). For the truncation K of the fitting model, we use $K = 1$ for the Q state and $K = 3$ for the rest. The local operator dual of each energy level is indicated on the left side, and the best-fit value is indicated by the parentheses. The red (blue) lines indicate the descendant operators from ϕ (T), whose positions are determined by the value of Δ_ϕ (Δ_T) that appears in the plot plus integers. The four primary operators are ϕ, $T_{\mu\nu}$, ϕ^3, and $Q_{\mu\nu\kappa\lambda}$.

$[\phi\phi]_{0,\ell}$ at spin 4, where the stress tensor also resides. We denote the spin-4 primary as $Q_{\mu\nu\kappa\lambda}$.

In Fig. 12, we take a closer look at the scalar primary operators ϕ and ϕ^3. We see that various fit truncation levels agree to a high precision. The small fluctuation of the extrapolation with respect to the fitting parameters provides us with a heuristic error bar, so we can determine

$$\Delta_\phi = 0.214(2), \qquad \Delta_{\phi^3} = 4.613(6). \tag{5.15}$$

We note that the fuzzy sphere result for Δ_ϕ is in excellent agreement with the high-temperature expansion result 0.214(6) from Ref. [60] and is also very close to our two-sided Padé estimate of approximately 0.218.

It is worth emphasizing that our confidence in the fuzzy sphere realization of the quantum criticality and the thermodynamic limit extrapolation is increased by the high precision agreement with conformal symmetry, which is presented in Fig. 13. The fact that the descendants of different spins agree with each other and are separated by integers is a result of the conformal algebra. We see that the agreement is generically broken for all states by a

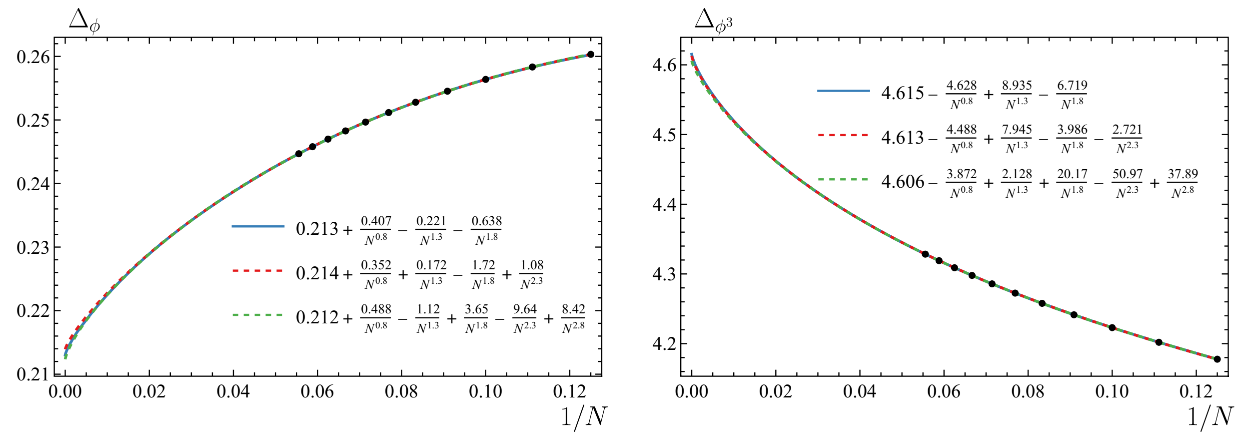

FIG. 12. Fitting various scaling dimensions with a range of fitting models. Left panel: scaling dimension of the lowest primary, the ϕ operator. Various powers converge to the same end value. Most fits agree up to within 0.002. Right panel: scaling dimension of the next-to-leading scalar primary, the ϕ^3 operator. Different fitting powers agree approximately up to a 0.006 error.

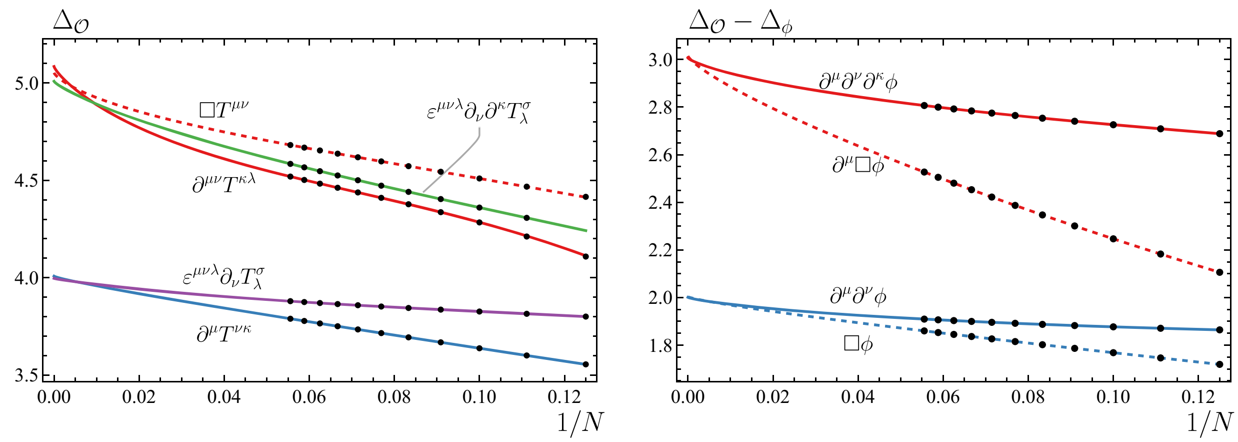

FIG. 13. Difference between several descendant states and their corresponding primary state. The agreement between $\Box = \partial_\mu\partial^\mu$ and $\partial^2 = (\partial_\mu\partial_\nu - \text{trace})$ relies on conformal symmetry. At finite N, they receive different finite-size corrections. We see that the extrapolation to $N \to \infty$ brings them all to integers.

significant amount at finite size, but the extrapolation brings them to the corresponding integers in a nonlinear manner. The agreement across many states is reached without any fine-tuning of fitting parameters. In Fig. 14, we utilize this property to determine the scaling dimension of the spin-4 primary $Q^{\mu\nu\kappa\lambda}$. As we move to the large spin regime, we inevitably find a denser spectrum. Indeed, there are three operators within a small domain $4.214 \leq \Delta \leq 5$: $\partial^\mu\partial^\nu\partial^\kappa\partial^\lambda\phi$, $\partial^\mu\partial^\nu T^{\kappa\lambda}$, and $Q^{\mu\nu\kappa\lambda}$. As a result, the fit to $\Delta_{Q^{\mu\nu\kappa\lambda}}$ is unstable. Instead, the spacetime parity-odd sector has a cleaner spectrum: There are no antisymmetric descendants of ϕ, and the leading operator in the spin-4 parity-odd sector is the antisymmetric descendant of Q, $\partial^{[\mu}Q^{\sigma]\nu\kappa\lambda}$. This operator has a healthier extrapolation, giving $\Delta_{\partial Q} = 5.9(1)$, and by conformal symmetry, it is expected to be exactly 1 above the primary scaling dimension. We conclude that

$$\Delta_{Q^{\mu\nu\kappa\lambda}} = 4.9(1). \tag{5.16}$$

Still, even in the parity-odd sector, ∂Q becomes dangerously close to $\partial^3 T$, and the possible mixing between the two levels may impact the accuracy of the fit.

Yang-Lee criticality has one relevant parameter, which means, in a phase diagram of more than one parameter, it will appear as a critical line or plane. In the phase diagram proposed in Fig. 5, we obtain a critical line where there is a critical coupling $ih_{z,c}$ for each h_x. Thus, we should obtain the same criticality for different h_x, and the extracted critical data should agree. In Fig. 15, we test the agreement of Δ_ϕ and the conformal algebra prediction $\Delta_{\partial^2\phi} - \Delta_\phi = 2$ for a range of h_x. The predictions from different h_x all agree when extrapolated to the thermodynamic limit, realizing the critical universality. We also see that large h_x is

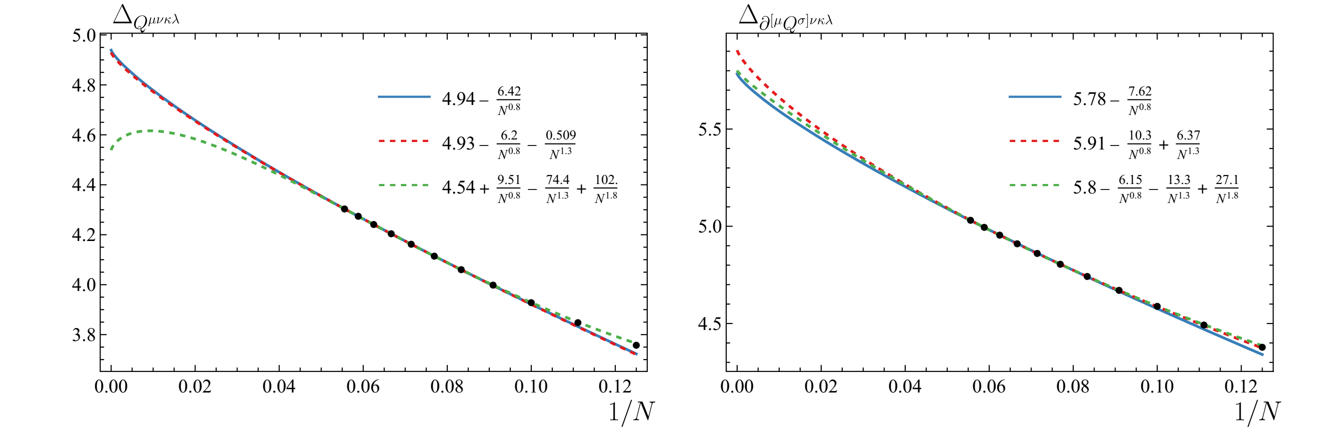

FIG. 14. Scaling dimension of the spin-4 primary $Q^{\mu\nu\kappa\lambda}$ and its antisymmetric descendant $\partial^{[\mu}Q^{\sigma]\nu\kappa\lambda}$. The latter operator is in the spacetime parity-odd sector and has no mixing with the descendant of ϕ, resulting in a better-behaved extrapolation.

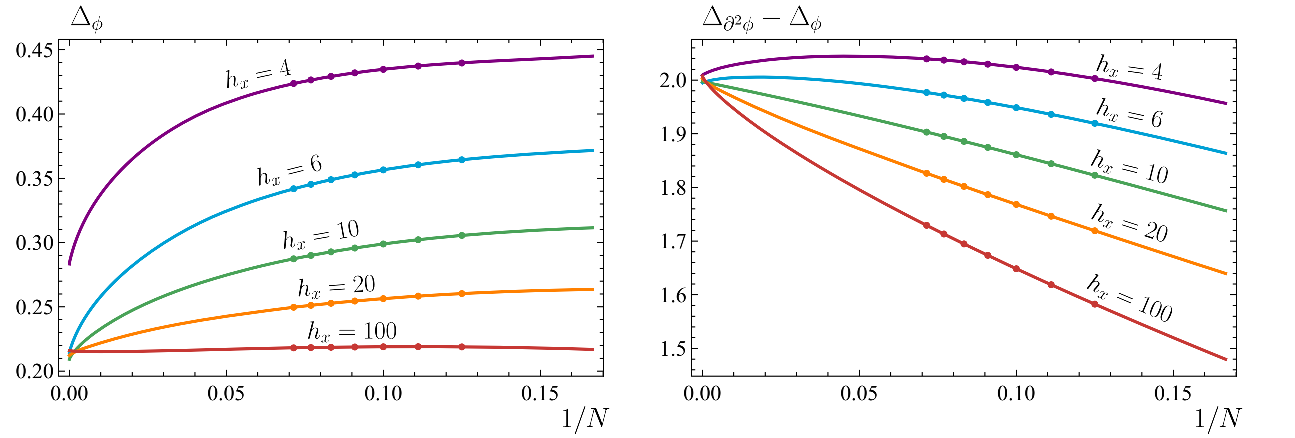

FIG. 15. Scaling dimension Δ_ϕ (left panel) and $\Delta_{\partial^2\phi} - \Delta_\phi$ (right panel) at the critical point of systems with various h_x couplings. The prediction from $N \to \infty$ extrapolations is stable for a wide range of h_x, indicating that they belong to the same universality class. The Δ_ϕ prediction from $h_x = 4$ deviates from the rest of the result by about 0.05, indicating that small h_x may be converging much more slowly than large h_x.

computationally favorable as it seems to receive smaller finite-size errors.

2. OPE coefficients

Apart from the operator scaling dimensions that encode the conformally invariant two-point function data, we are also interested in the OPE coefficients that encode the conformally invariant three-point function data. The most convenient way to extrapolate such information is through state-operator correspondence and by studying the fuzzy sphere matrix elements of the form

$$\langle \mathcal{O}_1, \ell_1, m_1 | M_{\ell_2 m_2} | \mathcal{O}_2, \ell_3, m_3 \rangle, \tag{5.17}$$

where $|\mathcal{O}, \ell, m\rangle$ is a fuzzy sphere matrix eigenstate in the spin (ℓ, m) sector and $M_{\ell_2 m_2}$ is a fuzzy sphere observable. The Yang-Lee Hamiltonian (5.5) is a complex symmetric operator; therefore, the left eigenvectors coincide with the right eigenvectors, $\langle \psi_i | = (|\psi_i\rangle)^T$. With this definition, we have $\langle \psi_i | \psi_j \rangle = \delta_{ij}$. In this work, we consider the following observables:

$$M^a_\ell = \frac{1}{2s+1} \int d^2\Omega Y_{\ell 0} \psi^\dagger(\Omega) \sigma^a \psi(\Omega),$$
$$X_\ell \equiv M^x_\ell, \qquad Z_\ell \equiv M^z_\ell, \tag{5.18}$$

where we suppress the quantum number m as we always work in the $m = 0$ representation. Unlike the quantum Ising model, there is no $\mathbb{Z}_2$ symmetry charge distinction between the X and Z operators; thus, they can generically have overlap with any operators, and the $\mathcal{PT}$ symmetry will determine the phase of the matrix elements. As discussed previously, each fuzzy sphere eigenstate can be identified as a CFT radial quantization eigenstate which is in one-to-one correspondence with a CFT local operator. The fuzzy sphere observable is much less determined. Note that $\psi^\dagger\sigma^a\psi$ is the local charge density operator in the UV, and it matches a generic linear combination of CFT local operators; the spherical smearing in Eq. (5.18) projects to modes with specific $SO(3)$ spin and flows to the most relevant operator in that sector in the thermodynamic limit

$$M^a_\ell = b_{a,0}\delta_{\ell,0}\mathbb{1} + b_{a,1}\int d^2\Omega Y_{\ell 0}(\Omega)\phi(\Omega) + \cdots, \quad (5.19)$$

where "$\cdots$" contains descendants and higher-dimensional primaries. We will study these matrix elements on a case-by-case basis.

We begin with scalar primary three-point functions. The scalar two-point and three-point functions are completely fixed by conformal symmetry,

$$\langle\mathcal{O}(x_1)\mathcal{O}(x_2)\rangle = \frac{1}{x_{12}^{2\Delta}}$$
$$\langle\mathcal{O}_1(x_1)\mathcal{O}_2(x_2)\mathcal{O}_3(x_3)\rangle = \frac{c_{123}}{x_{12}^{\Delta_1+\Delta_2-\Delta_3}x_{23}^{\Delta_2+\Delta_3-\Delta_1}x_{31}^{\Delta_3+\Delta_1-\Delta_2}}. \quad (5.20)$$

The state-operator correspondence in the scalar case is

$$|\mathcal{O},0\rangle = \lim_{x\to 0}\mathcal{O}(x)|0\rangle,$$
$$\langle\mathcal{O},0| = \lim_{x\to\infty} x^{2\Delta}\langle 0|\mathcal{O}(x). \quad (5.21)$$

Thus, the fuzzy sphere matrix element matches the scalar three-point function as

$$\langle\mathcal{O}_1,0|M^a_0|\mathcal{O}_3,0\rangle \supset \lim_{\substack{x_1\to\infty\\ x_3\to 0}} x_1^{2\Delta_1}\int d^2\Omega Y_{\ell 0}(\Omega)\langle O_1(x_1)O_2(\Omega)O_3(x_3)\rangle. \quad (5.22)$$

Thus, the expansion is

$$\langle\mathcal{O}_1,0|M^a_0|\mathcal{O}_3,0\rangle = b_0\delta_{\mathcal{O}_1\mathcal{O}_3} + b_1 C_{\mathcal{O}_1\phi\mathcal{O}_3} + \cdots, \quad (5.23)$$

and we can determine the OPE coefficient $C_{\phi\phi\phi}$ as

$$C_{\phi\phi\phi} = \frac{\langle\phi,0|M^a_0|\phi,0\rangle - \langle 0|M^a_0|0\rangle}{\langle 0|M^a_0|\phi,0\rangle} + O(N^{-1}). \quad (5.24)$$

The leading error term contains the contribution from the descendant $\partial^k\phi$. Only even powers can contribute to preserve spacetime parity. By dimensional analysis, the leading error $\partial^2\phi$ is suppressed by $R^{-2}\sim N^{-1}$. Similarly, $C_{\phi^3\phi\phi^3}$ can be determined by simply replacing the state ϕ by state ϕ^3. An off-diagonal matrix element is given by

$$C_{\mathcal{O}\phi\mathcal{O}'} = \frac{\langle\mathcal{O},0|M^a_0|\mathcal{O}',0\rangle}{\langle 0|M^a_0|\phi,0\rangle} + O(N^{-1}), \quad (5.25)$$

and we can use it to determine $C_{\phi\phi\phi^3}$. The numerical results of these scalar OPE coefficients are shown in Fig. 16. The predictions are [95]

$$|C_{\phi\phi\phi}| = 1.9696(31)_{[Z]}, \qquad 1.969(5)_{[X]},$$
$$|C_{\phi\phi\phi^3}| = 0.026(7)_{[Z]}, \qquad 0.0238(15)_{[X]},$$
$$|C_{\phi\phi^3\phi^3}| = 1.3774(9)_{[Z]}, \qquad 1.364(7)_{[X]}. \quad (5.26)$$

Next, we study the descendants of scalar primaries. The matching between fuzzy sphere states to such descendant states is

$$|\partial^k\mathcal{O},\ell\rangle \equiv a_{\mathcal{O},k,\ell}v_{\ell 0}^{\mu_1\cdots\mu_k}P_{\mu_1}\cdots P_{\mu_k}|\mathcal{O},0\rangle, \quad (5.27)$$

where P_μ is a conformal generator of translation, $v_{\ell 0}^{\mu_1\cdots\mu_k}$ is a vector projecting the 3^k tensor components to the $(\ell,0)$ representation of $SO(3)$, and $a_{\mathcal{O},k,\ell}$ is a normalization factor to keep the state normalized to 1. The matrix elements involving the descendants are completely determined by the conformal algebra up to the corresponding primary data. A number of useful diagonal matrix elements have been computed in Refs. [17,18],

$$A_{k,\ell}(\Delta,\Delta') \equiv \frac{\langle\partial^k\mathcal{O}',\ell|\int d^2\Omega Y_{00}(\Omega)\mathcal{O}(\Omega)|\partial^k\mathcal{O}',\ell\rangle}{\langle\mathcal{O}',0|\int d^2\Omega Y_{00}(\Omega)\mathcal{O}(\Omega)|\mathcal{O}',0\rangle}, \quad (5.28)$$

$$A_{1,1} = 1 + \frac{\mathcal{C}_\mathcal{O}}{6\Delta'}, \qquad \mathcal{C}_\mathcal{O} \equiv \Delta(\Delta-3). \quad (5.29)$$

Note that $A_{1,1}$ for $\mathcal{O}=\mathcal{O}'=\phi$ is a simple linear function of Δ_ϕ, and the right-hand side of Eq. (5.28) can be explicitly computed from the fuzzy sphere; thus, as an application, we use Eq. (5.28) to determine Δ_ϕ,

$$\Delta_\phi = 6\frac{\langle\partial\phi|M^a_0|\partial\phi\rangle - \langle 0|M^a_0|0\rangle}{\langle\phi|M^a_0|\phi\rangle - \langle 0|M^a_0|0\rangle} - 3. \quad (5.30)$$

The result is shown in Fig. 17. We obtain a prediction of the Δ_ϕ as

$$\Delta_\phi = 0.2155(16)_{[Z]}, \qquad 0.2151(8)_{[X]}. \quad (5.31)$$

It is remarkable that the Δ_ϕ determined in this way has a significantly smaller finite-size error. Indeed, the subleading terms in M^a_0 have a special feature. We expand it more to include the descendants of ϕ,

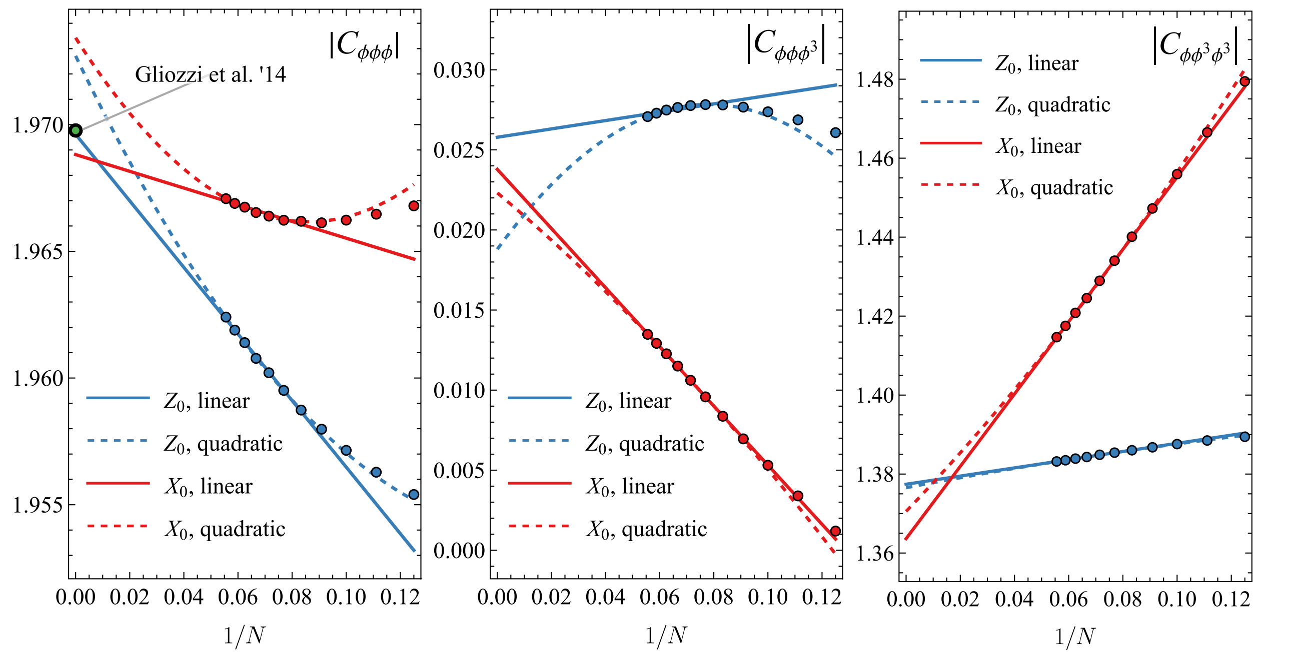

FIG. 16. Scalar OPE coefficients $C_{\phi\phi\phi}$, $C_{\phi\phi\phi^3}$, and $C_{\phi^3\phi\phi^3}$ measured from the fuzzy sphere data using the formulas (5.24) and (5.25). Blue (red) represents the Z_0 (X_0) observable, and the solid (dashed) lines represent the fit model $a + b/N$ ($a + b/N + c/N^2$). The $C_{\phi\phi\phi}$ measurement is compared with an earlier result obtained by solving truncated crossing equations [45,46].

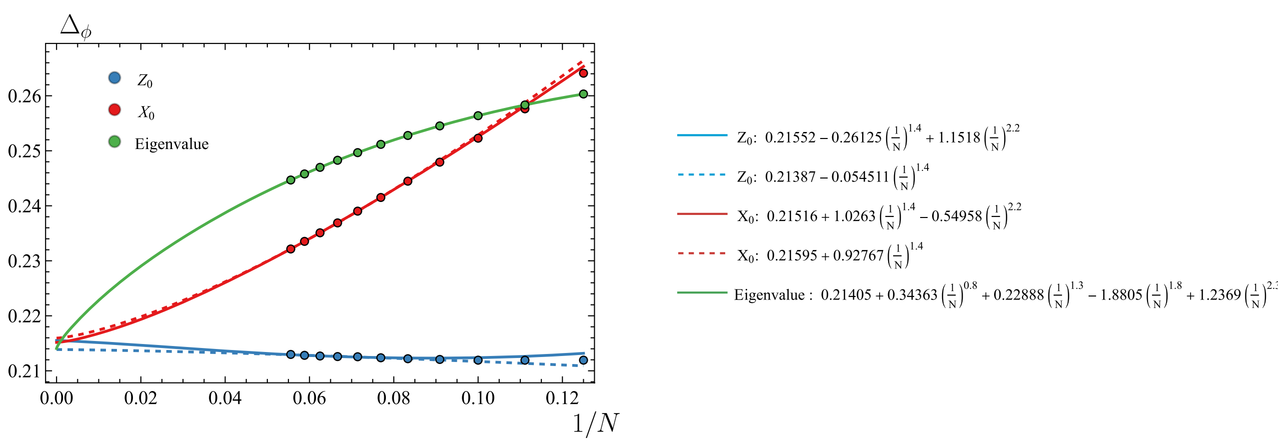

FIG. 17. Alternative determination of Δ_ϕ from the ratio of three-point functions, Eq. (5.30).

$$M_0^a = b_{a,0}\mathbb{1} + b_{a,1}\int d^2\Omega Y_{00}(\Omega)\phi(\Omega) + \sum_k b_{a,1}^{(k)}\int d^2\Omega Y_{00}(\Omega)\partial_r^k\phi(\Omega) + (\text{more primaries}\cdots). \tag{5.32}$$

Note that the spatial total derivatives have to vanish due to the integral against $Y_{00}(\Omega)$ over all the sphere, so the nonvanishing descendants can only be radial descendants. The action of k-fold radial derivatives has a simple pattern,

$$\partial_r^k \frac{1}{r^{\Delta_2+\Delta_3-\Delta_1}} = \frac{(-1)^k(\Delta_2+\Delta_3-\Delta_1)_k}{r^{\Delta_2+\Delta_3-\Delta_1+k}}, \tag{5.33}$$

where $(a)_k = \{[\Gamma(a+k)]/[\Gamma(a)]\}$ is the Pochammer symbol. Thus, all the descendants of ϕ terms can be resummed,

$$M_0^a = b_{a,0}\mathbb{1} + \left(b_{a,1} + \sum_{k=2}(-1)^k b_{a,1}^{(k)}(\Delta_\phi)_k\right)\int d^2\Omega Y_{00}(\Omega)\phi(\Omega) + (\text{more primaries}\cdots). \tag{5.34}$$

Now, note that the resummed coefficient is exactly the same when the external state is $\partial\phi$ instead of ϕ, so the ratio in Eq. (5.30) eliminates all errors up to the next primary operator $T^{\mu\nu}$. Thus, we expect the leading finite volume error to be $O(N^{-(d-\Delta_\phi)/2}) = O(N^{-1.4})$, whose convergence is much faster than the eigenvalues with $N^{-0.8}$ error. This finding qualitatively explains why the three-point function gives a better Δ_ϕ. We can also try using the fit to account for the next error, which is $N^{-2.2}$, given by the ϕ^3 contribution.

We conclude this section with an example of a scalar-spin-spin three-point function. In our convention, we normalize a generic spin-ℓ primary to have a two-point function of the standard form

$$\langle\mathcal{O}(x_1,z_1)\mathcal{O}(x_2,z_2)\rangle = \frac{((z_1\cdot z_2)-(x_{12}\cdot z_1)(x_{12}\cdot z_2)/x_{12}^2)^\ell}{x_{12}^{2\Delta}}, \tag{5.35}$$

where $x_{ij} = x_i - x_j$ and z_i^μ is an auxiliary vector introduced to keep the notation index-free: $\mathcal{O}(z) \equiv \mathcal{O}^{\mu_1\cdots\mu_\ell} z_{\mu_1}\cdots z_{\mu_\ell}$. A generic scalar-spin-spin correlator can have several polarizations carrying independent OPE coefficients. We follow the argument of Refs. [96,97] and expand the correlator as (assuming parity even)

$$\langle\mathcal{O}_1(x_1,z_1)\phi(x_2)\mathcal{O}_3(x_3,z_3)\rangle = \sum_{\substack{s=|\ell_1-\ell_3| \\ s-|\ell_1-\ell_3|=0 \bmod 2}}^{\ell_1+\ell_3} C^{(s)}_{\mathcal{O}_1\phi\mathcal{O}_3}\frac{H_{13}^{\frac{1}{2}(\ell_1+\ell_3-s)}V_{1,2,3}^{\frac{1}{2}(\ell_1-\ell_3+s)}V_{3,1,2}^{\frac{1}{2}(-\ell_1+\ell_3+s)}}{x_{12}^{\kappa_1+\kappa_2-\kappa_3}x_{13}^{\kappa_1+\kappa_3-\kappa_2}x_{23}^{\kappa_2+\kappa_3-\kappa_1}}, \tag{5.36}$$

where $\kappa_i = \Delta_i + \ell_i$, $x_{ij} = x_i - x_j$, and

$$H_{ij} = x_{ij}^2(z_i\cdot z_j) - 2(x_{ij}\cdot z_i)(x_{ij}\cdot z_j),$$
$$V_{i,j,k} = \frac{x_{ij}^2(x_{ik}\cdot z_i) - x_{ik}^2(x_{ij}\cdot z_i)}{x_{jk}^2}. \tag{5.37}$$

In this basis, the correspondence between the fuzzy sphere matrix elements and the OPE coefficients is

$$\langle\mathcal{O},\ell|M_s^a|\mathcal{O}',\ell'\rangle = \delta_{\mathcal{O},\mathcal{O}'}\delta_{s,0}b_0 + \sum_{s'} b_{a,1}f_{\ell,\ell',s,s'}C^{(s')}_{\mathcal{O}\phi\mathcal{O}'} + \cdots, \tag{5.38}$$

where $f_{\ell,\ell',s}$ is an exactly computable prefactor that only depends on the spins. The detailed derivation of this correspondence is included in Appendix B. With this convention, we study the $\langle\phi TT\rangle$ correlator, which has three polarizations, $s = 0$, 2, 4. The result is shown in Fig. 18. For $s = 0$, the convergence is good, and by extrapolating to the thermodynamic limit, we obtain

$$C^{(0)}_{\phi TT} = 1.157(2)_{[Z]}, \qquad 1.141(14)_{[X]}. \tag{5.39}$$

The error bar of the quantities is determined by the difference between the linear and quadratic fits. The fact that the two results differ by a gap greater than the error bar means the higher powers in $1/N$ still contribute significantly. As s become larger, the convergence becomes worse. A remarkable feature of the stress-tensor correlator is that the stress tensor is a conserved current, $\partial_\mu T^{\mu\nu} = 0$, which generates additional equations of motion that relate the OPE coefficients of different polarizations. It turns out that this correlator only has one independent OPE coefficient [97],

$$C^{(2)}_{\phi TT} = -\frac{2\Delta_\phi(\Delta_\phi-4)}{\Delta_\phi^2-6\Delta_\phi+6}C^{(0)}_{\phi TT},$$
$$C^{(4)}_{\phi TT} = \frac{\Delta_\phi(\Delta_\phi+2)}{2(\Delta_\phi^2-6\Delta_\phi+6)}C^{(0)}_{\phi TT}. \tag{5.40}$$

The conservation condition provides a nontrivial check of the conformal symmetry. Figure 18 shows that the fuzzy sphere data for $C^{(2)}_{\phi TT}$ and $C^{(4)}_{\phi TT}$ are in approximate agreement with conservation, and they converge to the theoretical values as N grows. Spinning correlators converge more slowly, and studying them thoroughly requires us to either push to higher N or implement more techniques to mitigate the finite-size error. We will leave this task as a future study.

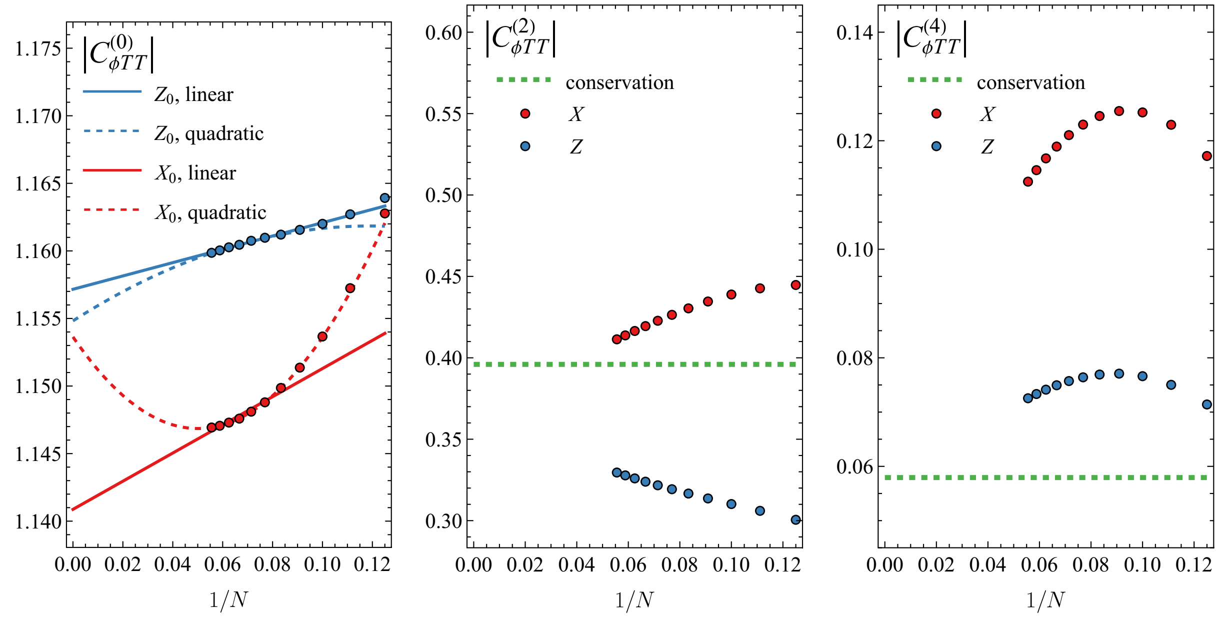

FIG. 18. Fuzzy sphere result of $C^{(s)}_{\phi TT}$ for $s = 0, 2, 4$.

VI. THE 4D MODEL ON THE 24-CELL (ICOSITETRACHORON)

The 24-cell or icositetrachoron is a self-dual regular 4D polytope (polychoron), which has $N = 24$ vertices and $E = 96$ edges. We can construct this polychoron by defining its vertices in a four-dimensional Cartesian coordinate system. Its 24 vertices v_i (for $i = 1, \ldots, 24$) are obtained by all permutations of coordinates of the vectors $(\pm 1, \pm 1, 0, 0)$. We draw the 24-cell as a graph on the F_4 Coxeter plane in Fig. 19.

The Yang-Lee Hamiltonian on the 24-cell reads

$$H_{\mathrm{YL}} = -J \sum_{\langle ij\rangle \in e} Z_i Z_j - h_x \sum_{i\in v} X_i - i h_z \sum_{i\in v} Z_i, \tag{6.1}$$

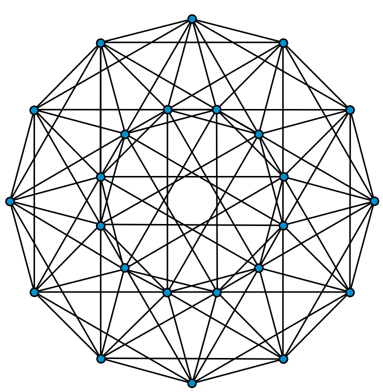

FIG. 19. Picture of the 24-cell as a graph on the F_4 Coxeter plane.

where the first sum is taken over all 96 edges and the last two sums are over the 24 vertices. The symmetry group of the 24-cell is the Weyl group of F_4, denoted as $W(F_4)$. This group has 1152 elements, 25 conjugacy classes, and 25 irreps [98–100]:

$$\mathbf{1}, \mathbf{1}', \mathbf{1}'', \mathbf{1}''', \mathbf{2}, \mathbf{2}', \mathbf{2}'', \mathbf{2}''', \mathbf{4}, \mathbf{4}', \mathbf{4}'', \mathbf{4}''', \mathbf{4}'''', \mathbf{6}, \mathbf{6}', \mathbf{8}, \mathbf{8}', \mathbf{8}'', \mathbf{8}''', \mathbf{9}, \mathbf{9}', \mathbf{9}'', \mathbf{9}''', \mathbf{12}, \mathbf{16}, \tag{6.2}$$

where the number represents an irrep's dimension. For convenience, we present the character table of $W(F_4)$ in Appendix A. The $O(4)$ irreps $(0, 0)$, $(1/2, 1/2)$, and $(1, 1)$ do not split on the 24-cell, and they correspond to irreps **1**, **4**, and **9**. The $O(4)$ irrep $(3/2, 3/2)$ splits into $\mathbf{8} + \mathbf{8}'$, $(2, 2)$ splits into $\mathbf{2} + \mathbf{2}' + \mathbf{9} + \mathbf{12}$, and $(5/2, 5/2)$ splits into $\mathbf{4} + \mathbf{8} + \mathbf{8}' + \mathbf{16}$.

We exhibit the lower energy gaps of the Hamiltonian (6.1) along the path $(h_x, ih_z) = (0, 0) \to (15, 0) \to (15, i6)$ with $J = 1$ in Fig. 20, where different colors correspond to different irreps of $W(F_4)$.

The behavior of the energy levels is similar to the 2D and 3D cases, and we can easily identify a few low-lying operators. We note that the 4D Ising model flows to a Gaussian fixed point in $d = 4$; for example, the operators ϕ, ϕ^2 should have dimensions $\Delta_\phi = 1$, $\Delta_{\phi^2} = 2$. However, due to finite-size corrections for the Ising model on the 24-cell, the energy gaps are shifted, and we do not observe the Gaussian fixed-point behavior for most of the levels; nevertheless, one can see that there is a pseudocritical point $h_x^* \approx 7.5$, where $\Delta_{\phi^2} \approx \Delta_{\partial\phi} \approx 2\Delta_\phi$. It would be

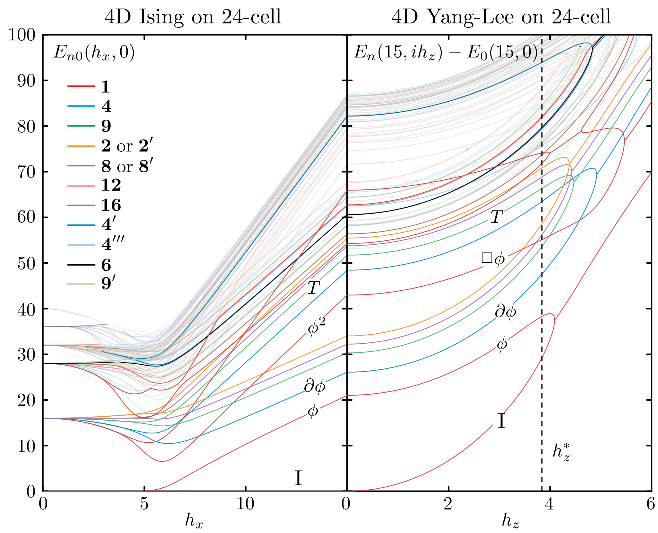

FIG. 20. Energy gaps of the Hamiltonian (6.1) for the 24-cell along the path $(h_x, ih_z) = (0, 0) \to (15, 0) \to (15, i6)$, with $J = 1$. We identified the lower energy levels with their corresponding operators in the Ising (Gaussian) and Yang-Lee CFTs. The dashed line is the pseudocritical point h_z^* obtained by fixing $r_T = 4$.

interesting to apply conformal perturbation theory to this model to better observe the Gaussian CFT behavior.

When the imaginary magnetic field ih_z is turned on, we observe a similar behavior for the energy gaps as in the 2D and 3D cases: the two lowest energy levels merge at some value ih_z^{merg}. We list the values of this merging point in Table XII.

To estimate the anomalous dimensions of the 4D Yang-Lee operators, we use the criticality criteria for pseudocritical point ih_z^*, which corresponds to fixing the ratio

$$r_T \equiv \frac{E_T - E_{\mathrm{I}}}{E_{\partial\phi} - E_\phi} \tag{6.3}$$

to be exactly $r_T = 4$. For the 24-cell, case corresponds to $r_T = (E_1^{(\mathbf{9})} - E_0^{(\mathbf{1})})/(E_0^{(\mathbf{4})} - E_1^{(\mathbf{1})})$. We list values ih_z^*, where $r_T = 4$, along with the anomalous dimensions of the scalar operators $\phi, \Box\phi, \Box^2\phi$, and ϕ^3 in Table XIII.

As in the 2D and 3D cases, we expect the finite-size corrections to be smaller for reasonably large h_x. We can see that at $h_x = 50$, the 24-cell result $\Delta_\phi \approx 0.891$ is within 8% from the Padé estimate $\Delta_\phi \approx 0.827$ (Table II); the latter is very close to the high-temperature expansion results [60]. The 24-cell result $\Delta_{\phi^3} \approx 5.467$ is within 5% from the Padé estimate $\Delta_{\phi^3} \approx 5.21$. We also notice that, as in 2D and 3D, the pseudocritical points ih_z^* obtained by fixing the ratio $r_T = 4$ are slightly away from the merging points listed in Table XII.

There are five other regular 4D polytopes one can consider: the 5-cell, 16-cell, 8-cell, 120-cell, and 600-cell. The 8-cell (hypercube) has only $N = 16$ vertices, so the 4D Yang-Lee or 4D Ising (Gaussian) models can be easily analyzed numerically on this polytope via exact diagonalization. On the other hand, the 120-cell and 600-cell have 600 and 120 vertices, respectively, making exact diagonalization unfeasible. However, modern numerical methods such as neural quantum states [101] could potentially be used to analyze the 4D Yang-Lee or 4D Ising models (the latter flows to the Gaussian one) on these large regular 4D polytopes. We leave this for future work.

VII. FUTURE DIRECTIONS

The methods we used for studying the quantum criticality of the Yang-Lee model in various dimensions can be used to calculate other observables in this nonunitary CFT. They include the entanglement entropy between the two hemispheres of S^{d-1}, as was done in Ref. [16] for the $d = 3$ Ising model. The latter can lead to the determination of the sphere free energy $\tilde{F}$ for the YL universality class, which may be compared with the results from the $6 - \epsilon$ expansion [102].

TABLE XII. Results for the merger points ih_z^{merg} of the Yang-Lee model on the 24-cell.

h_x	15	20	30	40	50	60	70	80	90	100
h_z^{merg}	4.090	7.470	15.021	23.135	31.572	40.222	49.025	57.945	66.956	76.042

TABLE XIII. Results for the anomalous dimensions $\Delta_\phi, \Delta_{\Box\phi}, \Delta_{\Box^2\phi}$, and Δ_{ϕ^3} at the pseudocritical point ih_z^* $(r_T = 4)$.

h_x	15	20	30	40	50	60	70	80	90	100
h_z^*	3.839	7.233	14.783	22.890	31.317	39.958	48.753	57.664	66.668	75.746
Δ_ϕ	0.976	0.944	0.914	0.900	0.891	0.886	0.881	0.878	0.876	0.874
$\Delta_{\Box\phi}$	2.796	2.876	2.951	2.987	3.009	3.023	3.034	3.042	3.049	3.054
$\Delta_{\Box^2\phi}$	4.593	4.607	4.638	4.658	4.672	4.682	4.691	4.697	4.702	4.707
Δ_{ϕ^3}	4.842	5.076	5.293	5.401	5.467	5.513	5.546	5.575	5.597	5.605

One of the new results in our paper is the use of the 24-cell to approximate the S^3. The results for the lowest operator dimension in $d = 4$ are quite good but not as precise as in $d = 3$. Obviously, it would be important to develop more precise methods for study the $d = 4$ YL CFT, such as a fuzzy S^3 where the size of the discretization can be varied.

We would also like to use similar methods to study other nonunitary universality classes. For example, the D_5 modular invariant of the minimal model $M(3, 8)$ has a Ginzburg-Landau description using a field theory of two scalar fields with cubic interactions containing imaginary coupling constants [68,70,103]. This model may be obtained by the RG flow from the D_6 modular invariant of $M(3, 10)$ [68,70,103–105], and the latter is a product of two Yang-Lee models [106,107]. It would be interesting to calculate observables in the $M(3, 8)$ universality class with the methods used in this paper and compare them with the $6 - \epsilon$ expansions and the exact results in $d = 2$.

Our work also provides useful input for future conformal bootstrap studies. For nonunitary CFTs, it is impossible to use the conventional convex optimization methods, but setups based on solving truncated crossing equations [45–47] can still be applied. Without positivity, this method is not rigorous; thus, one needs to start with a guess of the qualitative structure of the solution, and the CFT data we provided in this paper will be useful in this respect. Remarkably, there are recent works [108,109] on five-point function bootstrap methods using the truncated crossing equation method, which successfully extracted spin OPE coefficients such as $C_{\phi TT}$ for the 3D Ising model. Such quantities can also be obtained from bootstrapping of the mixed $\phi - T$ four-point functions system, which was recently done in Ref. [110]. Combining our results with these bootstrap techniques can hopefully improve our understanding of nonunitary CFTs.

Note added. Some of the preliminary results from this project were presented by one of us (G.T.) at the PCTS workshop “Spheres of Influence” [111]. Recently, we learned of two papers in preparation on related subjects [112,113].

ACKNOWLEDGMENTS

We are grateful to Richard Brower, Liam Fitzpatrick, Simone Giombi, Mina Himwich, Yin-Chen He, Luca Iliesiu, Andrei Katsevich, Yue-Zhou Li, Max Metlitski, David Poland, Zimo Sun, Matthew Walters, Zheng Zhou, and Yijian Zou for useful discussions. We also thank the participants of the Princeton Center for Theoretical Science workshop “Spheres of Influence” for stimulating interactions. Some of this research was carried out during the Kavli Institute for Theoretical Physics (KITP) workshop “Lattice and Continuum Approaches to Strongly Coupled QFT” and supported in part by Grant No. NSF PHY-2309135 to KITP. The work of E. A. C., G. T., and Y. X. was supported in part by the the U.S. Department of Energy (DOE) under Grant No. DE-SC0010118 and by the Simons Foundation under Grant No. 994316. The work of I. R. K. was supported in part by the U.S. National Science Foundation (NSF) under Grant No. PHY-2209997 and by the Simons Foundation under Grant No. 917464.

DATA AVAILABILITY

The data that support the findings of this article are not publicly available. The data are available from the authors upon reasonable request.

APPENDIX A: CHARACTERS OF $W(F_4)$

We denote representatives of the conjugacy classes of $W(F_4)$ by R_{q_L,q_R} for proper rotations and by $\tilde{R}_{q_L,q_R}$ for improper rotations [114], where q_L and q_R are two unit quaternions: $qq^\dagger = \sum_{i=0}^{3} q_i^2 = 1$, where $q = q_0 + q_1\mathbf{i} + q_2\mathbf{j} + q_3\mathbf{k}$, $q^\dagger = q_0 - q_1\mathbf{i} - q_2\mathbf{j} - q_3\mathbf{k}$, and $\mathbf{i}^2 = \mathbf{j}^2 = \mathbf{k}^2 = \mathbf{i}\,\mathbf{j}\mathbf{k} = -1$. The actions of the proper rotation R_{q_L,q_R} and the improper rotation $\tilde{R}_{q_L,q_R}$ on a vector $q = (q_0, q_1, q_2, q_3)$ in 4D space, represented as a quaternion, are

$$R_{q_L,q_R}(q) = q_L q q_R^\dagger, \qquad \tilde{R}_{q_L,q_R}(q) = q_L q^\dagger q_R^\dagger. \tag{A1}$$

The explicit expressions for the unit quaternions $q_1, q_2, \ldots q_8$ that define the representatives of the conjugacy classes of $W(F_4)$ are [114]

$$\begin{aligned} &q_1 = (1, 0, 0, 0), \qquad q_2 = (1, 0, 0, 0), \\ &q_4 = (0, 0, 1, 1)/\sqrt{2}, \qquad q_5 = (1, 0, 0, 1)/\sqrt{2}, \\ &q_6 = (1, 1, 0, 0)/\sqrt{2}, \qquad q_7 = (1, 1, 1, 1)/2, \\ &q_8 = (1, -1, -1, -1)/2. \end{aligned} \tag{A2}$$

The characters of $W(F_4)$ were computed in Ref. [98] (see also Refs. [100,115]). We present the characters of $W(F_4)$ for the proper rotations in Table XIV and for the improper rotations in Table XV.

TABLE XIV. Characters of $W(F_4)$ (proper rotations).

Conjugacy class	1	$4A_1$	$2A_1$	A_2	D_4	$D_4(a_1)$	$\tilde{A}_2$	C_3+A_1	$A_2+\tilde{A}_2$	$F_4(a_1)$	F_4	$A_1+\tilde{A}_1$	B_2	$A_3+\tilde{A}_1$	B_4
Size	1	1	18	32	32	12	32	32	16	16	96	72	36	36	144
Representative	R_{q_1,q_1}	$R_{q_1,-q_1}$	$R_{q_2,-q_2}$	R_{q_7,q_7}	$R_{q_7,-q_7}$	R_{q_2,q_1}	R_{q_7,q_8}	$R_{q_7,-q_8}$	$R_{q_7,-q_1}$	R_{q_7,q_1}	R_{q_2,q_7}	R_{q_4,q_4}	R_{q_6,q_6}	$R_{q_6,-q_6}$	$R_{q_6,-q_4}$
$\mathbf{1}(\phi_{1,0})$	1	1	1	1	1	1	1	1	1	1	1	1	1	1	1
$\mathbf{1}'(\phi''_{1,12})$	1	1	1	1	1	1	1	1	1	1	1	−1	−1	−1	−1
$\mathbf{1}''(\phi'_{1,12})$	1	1	1	1	1	1	1	1	1	1	1	−1	−1	−1	−1
$\mathbf{1}'''(\phi_{1,24})$	1	1	1	1	1	1	1	1	1	1	1	1	1	1	1
$\mathbf{2}(\phi''_{2,4})$	2	2	2	2	2	2	−1	−1	−1	−1	−1	0	0	0	0
$\mathbf{2}'(\phi'_{2,4})$	2	2	2	−1	−1	2	2	2	−1	−1	−1	0	0	0	0
$\mathbf{2}''(\phi'_{2,16})$	2	2	2	2	2	2	−1	−1	−1	−1	−1	0	0	0	0
$\mathbf{2}'''(\phi''_{2,16})$	2	2	2	−1	−1	2	2	2	−1	−1	−1	0	0	0	0
$\mathbf{4}(\phi_{4,13})$	4	−4	0	1	−1	0	1	−1	−2	2	0	0	2	−2	0
$\mathbf{4}'(\phi_{4,8})$	4	4	4	−2	−2	4	−2	−2	1	1	1	0	0	0	0
$\mathbf{4}''(\phi_{4,1})$	4	−4	0	1	−1	0	1	−1	−2	2	0	0	2	−2	0
$\mathbf{4}'''(\phi''_{4,7})$	4	−4	0	1	−1	0	1	−1	−2	2	0	0	−2	2	0
$\mathbf{4}'''(\phi'_{4,7})$	4	−4	0	1	−1	0	1	−1	−2	2	0	0	−2	2	0
$\mathbf{6}(\phi'_{6,6})$	6	6	−2	0	0	2	0	0	3	3	−1	2	−2	−2	0
$\mathbf{6}'(\phi''_{6,6})$	6	6	−2	0	0	2	0	0	3	3	−1	−2	2	2	0
$\mathbf{8}(\phi'_{8,9})$	8	−8	0	2	−2	0	−1	1	2	−2	0	0	0	0	0
$\mathbf{8}'(\phi''_{8,9})$	8	−8	0	−1	1	0	2	−2	2	−2	0	0	0	0	0
$\mathbf{8}''(\phi''_{8,3})$	8	−8	0	2	−2	0	−1	1	2	−2	0	0	0	0	0
$\mathbf{8}'''(\phi'_{8,3})$	8	−8	0	−1	1	0	2	−2	2	−2	0	0	0	0	0
$\mathbf{9}(\phi_{9,2})$	9	9	1	0	0	−3	0	0	0	0	0	1	1	1	−1
$\mathbf{9}'(\phi''_{9,6})$	9	9	1	0	0	−3	0	0	0	0	0	−1	−1	−1	1
$\mathbf{9}''(\phi'_{9,6})$	9	9	1	0	0	−3	0	0	0	0	0	−1	−1	−1	1
$\mathbf{9}'''(\phi_{9,10})$	9	9	1	0	0	−3	0	0	0	0	0	1	1	1	−1
$\mathbf{12}(\phi_{12,4})$	12	12	−4	0	0	4	0	0	−3	−3	1	0	0	0	0
$\mathbf{16}(\phi_{16,1})$	16	−16	0	−2	2	0	−2	2	−2	2	0	0	0	0	0

TABLE XV. Characters of $W(F_4)$ (improper rotations).

Conjugacy class	A_1	$3A_1$	$\tilde{A}_2+A_1$	C_3	A_3	$\tilde{A}_1$	$2A_1+\tilde{A}_1$	$A_2+\tilde{A}_1$	B_3	B_2+A_1
Size	12	12	96	96	72	12	12	96	96	72
Representative	$\tilde{R}_{q_4,-q_4}$	$\tilde{R}_{q_4,q_4}$	$\tilde{R}_{q_6,-q_5}$	$\tilde{R}_{q_6q_5}$	$\tilde{R}_{q_6,q_4}$	$\tilde{R}_{q_1q_1}$	$\tilde{R}_{q_2q_2}$	$\tilde{R}_{q_2q_7}$	$\tilde{R}_{q_7q_1}$	$\tilde{R}_{q_2q_1}$
$\mathbf{1}(\phi_{1,0})$	1	1	1	1	1	1	1	1	1	1
$\mathbf{1}'(\phi''_{1,12})$	1	1	1	1	1	−1	−1	−1	−1	−1
$\mathbf{1}''(\phi'_{1,12})$	−1	−1	−1	−1	−1	1	1	1	1	1
$\mathbf{1}'''(\phi_{1,24})$	−1	−1	−1	−1	−1	−1	−1	−1	−1	−1
$\mathbf{2}(\phi''_{2,4})$	2	2	−1	−1	2	0	0	0	0	0
$\mathbf{2}'(\phi'_{2,4})$	0	0	0	0	0	2	2	−1	−1	2
$\mathbf{2}''(\phi'_{2,16})$	−2	−2	1	1	−2	0	0	0	0	0
$\mathbf{2}'''(\phi''_{2,16})$	0	0	0	0	0	−2	−2	1	1	−2
$\mathbf{4}(\phi_{4,13})$	−2	2	1	−1	0	−2	2	1	−1	0
$\mathbf{4}'(\phi_{4,8})$	0	0	0	0	0	0	0	0	0	0
$\mathbf{4}''(\phi_{4,1})$	2	−2	−1	1	0	2	−2	−1	1	0
$\mathbf{4}'''(\phi''_{4,7})$	2	−2	−1	1	0	−2	2	1	−1	0
$\mathbf{4}'''(\phi'_{4,7})$	−2	2	1	−1	0	2	−2	−1	1	0

(Table continued)

TABLE XV. *(Continued)*

Conjugacy class	A_1	$3A_1$	$\tilde{A}_2+A_1$	C_3	A_3	$\tilde{A}_1$	$2A_1+\tilde{A}_1$	$A_2+\tilde{A}_1$	B_3	B_2+A_1
Size	12	12	96	96	72	12	12	96	96	72
Representative	$\tilde{R}_{q_4,-q_4}$	$\tilde{R}_{q_4,q_4}$	$\tilde{R}_{q_6,-q_5}$	$\tilde{R}_{q_6q_5}$	$\tilde{R}_{q_6,q_4}$	$\tilde{R}_{q_1q_1}$	$\tilde{R}_{q_2q_2}$	$\tilde{R}_{q_2q_7}$	$\tilde{R}_{q_7q_1}$	$\tilde{R}_{q_2q_1}$
$\mathbf{6}(\phi'_{6,6})$	0	0	0	0	0	0	0	0	0	0
$\mathbf{6}'(\phi''_{6,6})$	0	0	0	0	0	0	0	0	0	0
$\mathbf{8}(\phi'_{8,9})$	−4	4	−1	1	0	0	0	0	0	0
$\mathbf{8}'(\phi''_{8,9})$	0	0	0	0	0	−4	4	−1	1	0
$\mathbf{8}''(\phi''_{8,3})$	4	−4	1	−1	0	0	0	0	0	0
$\mathbf{8}'''(\phi'_{8,3})$	0	0	0	0	0	4	−4	1	−1	0
$\mathbf{9}(\phi_{9,2})$	3	3	0	0	−1	3	3	0	0	−1
$\mathbf{9}'(\phi''_{9,6})$	3	3	0	0	−1	−3	−3	0	0	1
$\mathbf{9}''(\phi'_{9,6})$	−3	−3	0	0	1	3	3	0	0	−1
$\mathbf{9}'''(\phi_{9,10})$	−3	−3	0	0	1	−3	−3	0	0	1
$\mathbf{12}(\phi_{12,4})$	0	0	0	0	0	0	0	0	0	0
$\mathbf{16}(\phi_{16,1})$	0	0	0	0	0	0	0	0	0	0

APPENDIX B: CONSTRUCTING SPINNING CORRELATION FUNCTIONS IN THE FUZZY SPHERE

In this appendix, we show an explicit construction of the spinning correlation functions using the fuzzy sphere observables. To fix our convention, we normalize the operators to have the standard form of the two-point function [8]

$$\langle \mathcal{O}(x_1,z_1)\mathcal{O}(x_2,z_2)\rangle = \frac{((z_1\cdot z_2)-(x_{12}\cdot z_1)(x_{12}\cdot z_2)/x_{12}^2)^\ell}{x_{12}^{2\Delta}} \tag{B1}$$

and three-point function [96,97]

$$\langle \mathcal{O}_1(x_1,z_1)\phi(x_2)\mathcal{O}_3(x_3,z_3)\rangle = \sum_{\substack{s=|\ell_1-\ell_3| \\ s-|\ell_1-\ell_3|=0 \bmod 2}}^{\ell_1+\ell_3} C^{(s)}_{\mathcal{O}_1\phi\mathcal{O}_3} \frac{H_{13}^{\frac{1}{2}(\ell_1+\ell_3-s)} V_{1,2,3}^{\frac{1}{2}(\ell_1-\ell_3+s)} V_{3,1,2}^{\frac{1}{2}(-\ell_1+\ell_3+s)}}{x_{12}^{\kappa_1+\kappa_2-\kappa_3} x_{13}^{\kappa_1+\kappa_3-\kappa_2} x_{23}^{\kappa_2+\kappa_3-\kappa_1}}, \tag{B2}$$

where $\kappa_i=\Delta_i+\ell_i$, $x_{ij}=x_i-x_j$. The building blocks are

$$\begin{aligned} H_{ij} &= (x_i-x_j)\cdot(x_i-x_j) z_i\cdot z_j - 2(x_i-x_j)\cdot z_i (x_i-x_j)\cdot z_j, \\ V_{i,j,k} &= \frac{(x_i-x_j)\cdot(x_i-x_j)(x_i-x_k)\cdot z_i - (x_i-x_k)\cdot(x_i-x_k)(x_i-x_j)\cdot z_i}{(x_j-x_k)\cdot(x_j-x_k)}. \end{aligned} \tag{B3}$$

The above formulas are in the index-free notation, and the indices can be recovered using the Todorov derivative

$$\begin{aligned} \mathcal{O}^{\mu_1\mu_2\cdots\mu_\ell}(x) &= \frac{1}{l!(1/2)_\ell} D_{z,\mu_1} D_{z,\mu_2}\cdots D_{z,\mu_\ell}\mathcal{O}(x,z), \\ D_{z,\mu} &= \left(\frac{d}{2}-1+z\cdot\frac{\partial}{\partial z}\right)\frac{\partial}{\partial z^\mu} - \frac{1}{2}z_\mu \frac{\partial^2}{\partial z\cdot\partial z}, \end{aligned} \tag{B4}$$

where $d=3$. We match the CFT radial quantization states to the fuzzy sphere states as

$$\begin{aligned} |\mathcal{O}_{\ell m}\rangle &= v^{\mu_1\mu_2\cdots\mu_\ell}_{\ell,\ell,m} \lim_{x\to 0}\mathcal{O}_{\mu_1\mu_2\cdots\mu_\ell}(x)|0\rangle \\ &\equiv \frac{(\mathbf{v}_{\ell,\ell,m}\cdot D_z^\ell)}{\ell!(1/2)_\ell}\lim_{x\to 0}\mathcal{O}(x,z)|0\rangle, \end{aligned} \tag{B5}$$

where the tensor $\mathbf{v}_{n,\ell,m}$ ($v^{\mu_1\mu_2\cdots\mu_\ell}_{\ell,\ell,m}$ being the component form) projects the tensor product of n indices to the (ℓ, m) representation. The vector is normalized to $\mathbf{v}\cdot\mathbf{v} = 1$. A construction of such vectors is shown below:

$$\mathbf{v}_{n,\ell,m} = \frac{1}{n}\sum_{k=0}^{n-1}\mathcal{R}^k(\mathbf{v}_{1,1,m'}\otimes\mathbf{v}_{n-1,|\ell-1|,m-m'})\langle|\ell-1|, m-m'; 1, m'|\ell, m\rangle, \tag{B6}$$

where $\mathcal{R}: f^{\mu_1\mu_2\cdots\mu_n}\mapsto f^{\mu_n\mu_1\cdots\mu_{n-1}}$ generates the cyclic permutation and $\mathcal{R}^k$ is permuting k times. Note that $\langle|\ell-1|, m-m'; 1, m'|\ell, m\rangle$ is the Clebsch-Gordan coefficient. The ket state is obtained from spatial inversion [9]:

$$\begin{aligned}\langle\mathcal{O}_{\ell m}| &= v^{\mu_1,\mu_2\cdots\mu_\ell}_{\ell,\ell,m}\lim_{x\to 0}x^{-2\Delta_\mathcal{O}}I_{\mu_1\nu_1}(x)I_{\mu_2\nu_2}(x)\cdots I_{\mu_\ell\nu_\ell}(x)\mathcal{O}^{\nu_1\nu_2\cdots\nu_\ell}\left(\frac{x}{|x|^2}\right)|0\rangle\\ &= \frac{(\mathbf{v}_{\ell,\ell,m}\cdot D_z^\ell)}{\ell!(1/2)_\ell}\lim_{x\to\infty}x^{2\Delta_\mathcal{O}}\mathcal{O}(x, z-2(x\cdot z)z)|0\rangle,\end{aligned} \tag{B7}$$

where $I_{\mu\nu} = \delta_{\mu\nu} - 2[(x_\mu x_\nu)/x^2]$. Strictly speaking, the ket state is not quite the conjugation, but the left eigenvector and the inversion will also take $\mathcal{O}\mapsto\mathcal{O}^\dagger$. In the YL model, the left and right eigenvectors are related by complex conjugation, which cancels the conjugation of the operator if it is not real. The net effect is that we do not need to worry about the conjugation of $\mathcal{O}$. By extrapolating $\mathcal{O}_1$ and $\mathcal{O}_3$ to ∞ and 0, we obtain a much cleaner expression,

$$\langle\mathcal{O}(z_1)|\mathcal{O}(x_2)|\mathcal{O}(z_3)\rangle \propto (z_1\cdot z_3)^{\frac{1}{2}(\ell_1+\ell_3-\ell_2)}(z_1\cdot x_2)^{\frac{1}{2}(\ell_1+\ell_2-\ell_3)}(z_3\cdot x_2)^{\frac{1}{2}(\ell_2+\ell_3-\ell_1)}. \tag{B8}$$

We match the leading behavior fuzzy sphere operator $M^a_{\ell m}$ to the integral of ϕ over the sphere weighted by spherical harmonics,

$$M^a_{\ell m} = b_{a,0}\delta_{\ell,0}\mathbb{1} + b_{a,1}\int d^2\Omega Y_{\ell m}(\Omega)\phi(\Omega) + \cdots, \tag{B9}$$

and this integral can be alternatively evaluated by contracting the spinning tensor indices to $\mathbf{v}$ tensors; however, this time the variable carrying the indices is the spatial coordinate x (which is also Ω),

$$\int d^2\Omega Y_{\ell m}(\Omega) = \alpha_\ell\frac{(\mathbf{v}_{n,\ell,m}\cdot\partial_x^n)}{n!\mathrm{Tr}(\mathbf{v}_{n,\ell,m}\cdot\mathbf{v}_{\ell,\ell,m})}, \qquad \alpha_\ell = \sqrt{\frac{4\pi(1/2)_\ell}{(1+2\ell)2^{-\ell}\ell!}}, \tag{B10}$$

which helps us to obtain the spin-dependent coefficient in the fuzzy sphere matrix element,

$$\begin{aligned}\langle\mathcal{O},\ell|M^a_s|\mathcal{O}',\ell'\rangle &= \delta_{\mathcal{O},\mathcal{O}'}\delta_{s,0}b_0 + \sum_{s'}b_{a,1}f_{\ell,\ell',s,s'}C^{(s')}_{\mathcal{O}\phi\mathcal{O}'} + \cdots\\ f_{\ell,\ell',s,s'} &= \alpha_s\frac{(\mathbf{v}_{s',s,0}\cdot\partial_{x_2}^{s'})}{s!\mathrm{Tr}(\mathbf{v}_{s',s,0}\cdot\mathbf{v}_{s,s,0})}\frac{(\mathbf{v}_{\ell,\ell,0}\cdot D_{z_1}^\ell)}{\ell!(1/2)_\ell}\frac{(\mathbf{v}_{\ell',\ell',0}\cdot D_{z_3}^{\ell'})}{\ell'!(1/2)_{\ell'}}(z_1\cdot z_3)^{\frac{1}{2}(\ell+\ell'-s')}(z_1\cdot x_2)^{\frac{1}{2}(\ell+s'-\ell')}(z_3\cdot x_2)^{\frac{1}{2}(s'+\ell'-\ell)}.\end{aligned} \tag{B11}$$

[1] E. Ising, *Contribution to the theory of ferromagnetism*, Z. Phys. **31**, 253 (1925).

[2] L. Onsager, *Crystal statistics. 1. A two-dimensional model with an order disorder transition*, Phys. Rev. **65**, 117 (1944).

[3] A. Belavin, A. M. Polyakov, and A. Zamolodchikov, *Infinite conformal symmetry in two-dimensional quantum field theory*, Nucl. Phys. **B241**, 333 (1984).

[4] K. G. Wilson and M. E. Fisher, *Critical exponents in 3.99 dimensions*, Phys. Rev. Lett. **28**, 240 (1972).

[5] R. Rattazzi, V. S. Rychkov, E. Tonni, and A. Vichi, *Bounding scalar operator dimensions in 4D CFT*, J. High Energy Phys. 12 (2008) 031.

[6] S. El-Showk, M. F. Paulos, D. Poland, S. Rychkov, D. Simmons-Duffin, and A. Vichi, *Solving the 3D Ising model with the conformal bootstrap*, Phys. Rev. D **86**, 025022 (2012).

[7] A. M. Polyakov, *Conformal symmetry of critical fluctuations*, JETP Lett. **12**, 381 (1970).

[8] D. Poland, S. Rychkov, and A. Vichi, *The conformal bootstrap: Theory, numerical techniques, and applications*, Rev. Mod. Phys. **91**, 015002 (2019).

[9] D. Simmons-Duffin, *The conformal bootstrap*, in *New Frontiers in Fields and Strings* (World Scientific, Singapore, 2017), pp. 1–74.

[10] S. Rychkov, *EPFL Lectures on Conformal Field Theory in D>=3 Dimensions*, SpringerBriefs in Physics (Springer, Geneva, 2016), 1.

[11] S. M. Chester, *Weizmann lectures on the numerical conformal bootstrap*, Phys. Rep. **1045**, 1 (2023).

[12] A. Cappelli, L. Maffi, and S. Okuda, *Critical Ising model in varying dimension by conformal bootstrap*, J. High Energy Phys. 01 (2019) 161.

[13] J. Henriksson, S. R. Kousvos, and M. Reehorst, *Spectrum continuity and level repulsion: The Ising CFT from infinitesimal to finite* ε, J. High Energy Phys. 02 (2023) 218.

[14] W. Zhu, C. Han, E. Huffman, J. S. Hofmann, and Y.-C. He, *Uncovering conformal symmetry in the 3D Ising transition: State-operator correspondence from a quantum fuzzy sphere regularization*, Phys. Rev. X **13**, 021009 (2023).

[15] L. Hu, Y.-C. He, and W. Zhu, *Operator product expansion coefficients of the 3D Ising criticality via quantum fuzzy spheres*, Phys. Rev. Lett. **131**, 031601 (2023).

[16] L. Hu, W. Zhu, and Y.-C. He, *Entropic F-function of 3D Ising conformal field theory via the fuzzy sphere regularization*, Phys. Rev. B **111**, 155151 (2025).

[17] B.-X. Lao and S. Rychkov, *3D Ising CFT and exact diagonalization on icosahedron: The power of conformal perturbation theory*, SciPost Phys. **15**, 243 (2023).

[18] A. M. Läuchli, L. Herviou, P. H. Wilhelm, and S. Rychkov, *Exact diagonalization, matrix product states and conformal perturbation theory study of a 3D Ising fuzzy sphere model*, SciPost Phys. **19**, 076 (2025).

[19] C. Han, L. Hu, W. Zhu, and Y.-C. He, *Conformal four-point correlators of the three-dimensional Ising transition via the quantum fuzzy sphere*, Phys. Rev. B **108**, 235123 (2023).

[20] F. D. M. Haldane, *Fractional quantization of the Hall effect: A hierarchy of incompressible quantum fluid states*, Phys. Rev. Lett. **51**, 605 (1983).

[21] J. Madore, *The fuzzy sphere*, Classical Quantum Gravity **9**, 69 (1992).

[22] G. Fardelli, A. L. Fitzpatrick, and E. Katz, *Constructing the infrared conformal generators on the fuzzy sphere*, SciPost Phys. **18**, 086 (2025).

[23] R. Fan, *Note on explicit construction of conformal generators on the fuzzy sphere*, arXiv:2409.08257.

[24] D. Przetakiewicz, S. Wessel, and F. P. Toldin, *Boundary operator product expansion coefficients of the three-dimensional Ising universality class*, Phys. Rev. Res. **7**, L032051 (2025).

[25] Z. Zhou and Y.-C. He, *A new series of 3D CFTs with* Sp(N) *global symmetry on fuzzy sphere*, Phys. Rev. Lett. **135**, 026504 (2025).

[26] M. Dedushenko, *Ising BCFT from fuzzy hemisphere*, arXiv:2407.15948.

[27] B.-B. Chen, X. Zhang, and Z. Yang Meng, *Emergent conformal symmetry at the multicritical point of* $(2+1)$D *SO(5) model with Wess-Zumino-Witten term on a sphere*, Phys. Rev. B **110**, 125153 (2024).

[28] B.-B. Chen, X. Zhang, Y. Wang, K. Sun, and Z. Y. Meng, *Phases of* $(2+1)$D *SO(5) nonlinear sigma model with a topological term on a sphere: Multicritical point and disorder phase*, Phys. Rev. Lett. **132**, 246503 (2024).

[29] Z. Zhou, L. Hu, W. Zhu, and Y.-C. He, *SO(5) deconfined phase transition under the fuzzy-sphere microscope: Approximate conformal symmetry, pseudo-criticality, and operator spectrum*, Phys. Rev. X **14**, 021044 (2024).

[30] C. Han, L. Hu, and W. Zhu, *Conformal operator content of the Wilson-Fisher transition on fuzzy sphere bilayers*, Phys. Rev. B **110**, 115113 (2024).

[31] D. L. Jafferis, I. R. Klebanov, S. S. Pufu, and B. R. Safdi, *Towards the F-theorem:* $\mathcal{N}=2$ *field theories on the three-sphere*, J. High Energy Phys. 06 (2011) 102.

[32] I. R. Klebanov, S. S. Pufu, and B. R. Safdi, *F-Theorem without supersymmetry*, J. High Energy Phys. 10 (2011) 038.

[33] H. Casini and M. Huerta, *On the RG running of the entanglement entropy of a circle*, Phys. Rev. D **85**, 125016 (2012).

[34] L. Fei, S. Giombi, I. R. Klebanov, and G. Tarnopolsky, *Generalized F-theorem and the* ϵ *expansion*, J. High Energy Phys. 12 (2015) 155.

[35] C.-N. Yang and T. D. Lee, *Statistical theory of equations of state and phase transitions. 1. Theory of condensation*, Phys. Rev. **87**, 404 (1952).

[36] T. D. Lee and C.-N. Yang, *Statistical theory of equations of state and phase transitions. 2. Lattice gas and Ising model*, Phys. Rev. **87**, 410 (1952).

[37] P. J. Kortman and R. B. Griffiths, *Density of zeros on the Lee-Yang circle for two Ising ferromagnets*, Phys. Rev. Lett. **27**, 1439 (1971).

[38] M. Fisher, *Yang-Lee edge singularity and* ϕ^3 *field theory*, Phys. Rev. Lett. **40**, 1610 (1978).

[39] J. L. Cardy, *Conformal invariance and the Yang-Lee edge singularity in two-dimensions*, Phys. Rev. Lett. **54**, 1354 (1985).

[40] J. Cardy, *The Yang-Lee edge singularity and related problems*, arXiv:2305.13288.

[41] M. Borinsky, J. A. Gracey, M. V. Kompaniets, and O. Schnetz, *Five-loop renormalization of* ϕ^3 *theory with applications to the Lee-Yang edge singularity and percolation theory*, Phys. Rev. D **103**, 116024 (2021).

[42] M. Kompaniets and A. Pikelner, *Critical exponents from five-loop scalar theory renormalization near six-dimensions*, Phys. Lett. B **817**, 136331 (2021).

[43] After the original version of this paper appeared, the six-loop beta function and anomalous dimension became available [44], which determine the $O(\epsilon^6)$ terms in Δ_ϕ and Δ_{ϕ^3}.

[44] O. Schnetz, ϕ^3 *theory at six loops*, Phys. Rev. D **112**, 016028 (2025).

[45] F. Gliozzi, *More constraining conformal bootstrap*, Phys. Rev. Lett. **111**, 161602 (2013).

[46] F. Gliozzi and A. Rago, *Critical exponents of the 3D Ising and related models from conformal bootstrap*, J. High Energy Phys. 10 (2014) 042.

[47] S. Hikami, *Conformal bootstrap analysis for the Yang–Lee edge singularity*, Prog. Theor. Exp. Phys. **2018**, 053I01 (2018).

[48] The icosahedron has also been used to discretize the 2D classical Ising model on a sphere [49,50].

[49] R. C. Brower and E. K. Owen, *The Ising model on* $\mathbb{S}^2$, arXiv:2407.00459.

[50] R. C. Brower, G. T. Fleming, N. Matsumoto, and R. Misra, *Ising on* $\mathbb{S}^2$*–The Affine Conjecture*, in *41st International Symposium on Lattice Field Theory* (2025), 3, arXiv:2503.05621.

[51] G. von Gehlen, *Critical and off critical conformal analysis of the Ising quantum chain in an imaginary field*, J. Phys. A **24**, 5371 (1991).

[52] G. von Gehlen, *NonHermitian tricriticality in the Blume-Capel model with imaginary field*, arXiv:hep-th/9402143.

[53] O. A. Castro-Alvaredo and A. Fring, *A spin chain model with non-Hermitian interaction: The Ising quantum spin chain in an imaginary field*, J. Phys. A **42**, 465211 (2009).

[54] More recent studies of non-Hermitian spin chain Hamiltonians were carried out in the context of Q-state Potts models with $Q = 5$ [55,56]. Let us also note that the YL universality class is related to the $Q \to \infty$ limit of the Potts model [57].

[55] Y. Tang, H. Ma, Q. Tang, Y.-C. He, and W. Zhu, *Reclaiming the lost conformality in a non-Hermitian quantum 5-state Potts model*, Phys. Rev. Lett. **133**, 076504 (2024).

[56] J. L. Jacobsen and K. J. Wiese, *Lattice realization of complex conformal field theories: Two-dimensional Potts model with* $Q > 4$ *states*, Phys. Rev. Lett. **133**, 077101 (2024).

[57] K. J. Wiese and J. L. Jacobsen, *The two upper critical dimensions of the Ising and Potts models*, J. High Energy Phys. 05 (2024) 092.

[58] K. Uzelac and R. Jullien, *The Yang-Lee edge singularity by the phenomenological renormalisation group*, J. Phys. A **14**, L151 (1981).

[59] E. Arguello Cruz, G. Tarnopolsky, and Y. Xin, *Precision study of the massive Schwinger model near quantum criticality*, Phys. Rev. D **112**, 034023 (2025).

[60] P. Butera and M. Pernici, *Yang-Lee edge singularities from extended activity expansions of the dimer density for bipartite lattices of dimensionality* 2 <= d <= 7, Phys. Rev. E **86**, 011104 (2012).

[61] V. P. Yurov and A. B. Zamolodchikov, *Truncated conformal space approach to scaling Lee-Yang model*, Int. J. Mod. Phys. A **05**, 3221 (1990).

[62] H.-L. Xu and A. Zamolodchikov, *2D Ising field theory in a magnetic field: The Yang-Lee singularity*, J. High Energy Phys. 08 (2022) 057.

[63] M. Leitner, *The (2,5) minimal model on genus two surfaces*, arXiv:1801.08387.

[64] A. Katsevich, *The spectrum of perturbed (3, 10) minimal model*, arXiv:2410.18069.

[65] C. M. Bender, N. Hassanpour, S. P. Klevansky, and S. Sarkar, *PT-symmetric quantum field theory in D dimensions*, Phys. Rev. D **98**, 125003 (2018).

[66] O. de Alcantara Bonfim, J. Kirkham, and A. McKane, *Critical exponents to order* ϵ^3 *for* ϕ^3 *models of critical phenomena in* $6-\epsilon$ *dimensions*, J. Phys. A **13**, L247 (1980).

[67] O. de Alcantara Bonfim, J. Kirkham, and A. McKane, *Critical exponents for the percolation problem and the Yang-Lee edge singularity*, J. Phys. A **14**, 2391 (1981).

[68] L. Fei, S. Giombi, I. R. Klebanov, and G. Tarnopolsky, *Three loop analysis of the critical O(N) models in* $6-\varepsilon$ *dimensions*, Phys. Rev. D **91**, 045011 (2015).

[69] This approach is analogous to the identification of $L_{-3}\bar{L}_{-3}\phi$ in the 2D Ising model $M(3,4)$ with the operator ϕ^5 in the massless ϕ^4 field theory [46].

[70] I. R. Klebanov, V. Narovlansky, Z. Sun, and G. Tarnopolsky, *Ginzburg-Landau description and emergent supersymmetry of the (3, 8) minimal model*, J. High Energy Phys. 02 (2023) 066.

[71] S. Giombi and V. Kirilin, *Anomalous dimensions in CFT with weakly broken higher spin symmetry*, J. High Energy Phys. 11 (2016) 068.

[72] R. Gopakumar, A. Kaviraj, K. Sen, and A. Sinha, *Conformal bootstrap in Mellin space*, Phys. Rev. Lett. **118**, 081601 (2017).

[73] P. Dey and A. Kaviraj, *Towards a bootstrap approach to higher orders of epsilon expansion*, J. High Energy Phys. 02 (2018) 153.

[74] V. Goncalves, *Skeleton expansion and large spin bootstrap for* ϕ^3 *theory*, arXiv:1809.09572.

[75] In the Ising model, the dimension of $T'_{\mu\nu}$ as a function of d was calculated using the numerical bootstrap methods [12]. It equals 6 in 4D and 2D, while in 3D it is approximately 5.5.

[76] S. Nixon and J. Yang, *Nonlinear wave dynamics near phase transition in PT-symmetric localized potentials*, Physica (Amsterdam) **331D**, 48 (2016).

[77] A. Chernyavsky and D. E. Pelinovsky, *Krein signature for instability of PT-symmetric states*, Physica (Amsterdam) **371D**, 48 (2018).

[78] G. A. Starkov, M. V. Fistul, and I. M. Eremin, *Formation of exceptional points in pseudo-Hermitian systems*, Phys. Rev. A **108**, 022206 (2023).

[79] Y.-J. Wei and Z.-C. Gu, *Tensor network renormalization: Application to dynamic correlation functions and non-hermitian systems*, arXiv:2311.18785.

[80] M. G. Yamada, T. Sanno, M. O. Takahashi, Y. Akagi, H. Suwa, S. Fujimoto, and M. Udagawa, *Matrix product renormalization group: Potential universal quantum many-body solver*, arXiv:2212.13267.

[81] W. D. Heiss, *The physics of exceptional points*, J. Phys. A **45**, 444016 (2012).

[82] C. J. Hamer and M. N. Barber, *Finite-size scaling in Hamiltonian field theory*, J. Phys. A **13**, L169 (1980).

[83] C. J. Hamer and M. N. Barber, *Finite-lattice methods in quantum Hamiltonian field theory. I. The Ising model*, J. Phys. A **14**, 241 (1981).

[84] C. J. Hamer and M. N. Barber, *Finite-lattice methods in quantum Hamiltonian field theory. I. O(2) and O(3) Heisenberg models*, J. Phys. A, **14** 259 (1981).

[85] G. Von Gehlen, *Critical and off-critical conformal analysis of the Ising quantum chain in an imaginary field*, J. Phys. A **24**, 5371 (1991).

[86] G. V. Gehlen, *Non-Hermitian tricriticality in the Blume-Capel model with imaginary field*, Int. J. Mod. Phys. B **08**, 3507 (1994).

[87] Although *CPT* predicts the convergence rate of $ih_z^*(N)$ to $ih_z^{\rm crit}$ at large N, we observe that, for small values of N, the points are fitted well by the $1/N$ linear fit.

[88] For the FSS criterion, we followed Ref. [82] and defined $h_z^*(N)$ as the point where

$$\sqrt{N+1}E_{10}^{(\mathbf{1})}(N+1) = \sqrt{N}E_{10}^{(\mathbf{1})}(N),$$

where we used $R \propto \sqrt{N}$ [89].

[89] Z. Zhou, *FuzzifiED: Julia package for numerics on the fuzzy sphere*, arXiv:2503.00100.

[90] J. L. Cardy, *Operator content of two-dimensional conformally invariant theories*, Nucl. Phys. **B270**, 186 (1986).

[91] A. B. Zamolodchikov, *Renormalization group and perturbation theory near fixed points in two-dimensional field theory*, Sov. J. Nucl. Phys. **46**, 1090 (1987).

[92] J. L. Cardy, *Conformal invariance and universality in finite-size scaling*, J. Phys. A **17**, L385 (1984).

[93] Y. Zou, A. Milsted, and G. Vidal, *Conformal data and renormalization group flow in critical quantum spin chains using periodic uniform matrix product states*, Phys. Rev. Lett. **121**, 230402 (2018).

[94] Y. Zou, A. Milsted, and G. Vidal, *Conformal fields and operator product expansion in critical quantum spin chains*, Phys. Rev. Lett. **124**, 040604 (2020).

[95] The error bars are determined by the difference between the linear and quadratic extrapolations. The purpose of these error bars is to show the scale of a possible fitting error but not to assert that the true value should lie within the error bar. Note that $C_{\phi\phi^3\phi^3}$ has nonoverlapping error bars.

[96] M. S. Costa, J. Penedones, D. Poland, and S. Rychkov, *Spinning conformal correlators*, J. High Energy Phys. 11 (2011) 071.

[97] D. Meltzer, *Higher spin ANEC and the space of CFTs*, J. High Energy Phys. 07 (2019) 001.

[98] T. Kondo, *The characters of the Weyl group of type F4*, J. Fac. Sci. Univ. Tokyo Sect. I **11**, 1965 (1965).

[99] R. W. Carter, *Conjugacy classes in the Weyl group*, Compos. Math. **25**, 1 (1972).

[100] R. Carter, *Finite Groups of Lie Type: Conjugacy Classes and Complex Characters*, Wiley Classics Library (Wiley, New York, 1993).

[101] G. Carleo and M. Troyer, *Solving the quantum many-body problem with artificial neural networks*, Science **355**, 602 (2017).

[102] S. Giombi, E. Himwich, A. Katsevich, I. Klebanov, and Z. Sun, *Sphere free energy of scalar field theories with cubic interactions*, arXiv:2412.14086.

[103] A. Katsevich, I. R. Klebanov, and Z. Sun, *Ginzburg-Landau description of a class of non-unitary minimal models*, J. High Energy Phys. 03 (2025) 170.

[104] Y. Nakayama and T. Tanaka, *Infinitely many new renormalization group flows between Virasoro minimal models from non-invertible symmetries*, J. High Energy Phys. 11 (2024) 137.

[105] O. Delouche, J. Elias Miro, and J. Ingoldby, *Testing the RG-flow $M(3,10)+\phi_{1,7}\to M(3,8)$ with Hamiltonian truncation*, J. High Energy Phys. 04 (2025) 144.

[106] H. Kausch, G. Takacs, and G. Watts, *On the relation between Phi(1,2) and Phi(1,5) perturbed minimal models*, Nucl. Phys. **B489**, 557 (1997).

[107] T. Quella, I. Runkel, and G. M. Watts, *Reflection and transmission for conformal defects*, J. High Energy Phys. 04 (2007) 095.

[108] D. Poland, V. Prilepina, and P. Tadić, *Improving the five-point bootstrap*, J. High Energy Phys. 05 (2024) 299.

[109] D. Poland, V. Prilepina, and P. Tadić, *The five-point bootstrap*, J. High Energy Phys. 10 (2023) 153.

[110] C.-H. Chang, V. Dommes, R. S. Erramilli, A. Homrich, P. Kravchuk, A. Liu, M. S. Mitchell, D. Poland, and D. Simmons-Duffin, *Bootstrapping the 3D Ising stress tensor*, J. High Energy Phys. 03 (2025) 136.

[111] G. Tarnopolsky, *Numerical analysis of the Yang-Lee critical point across different dimensions*, Available from https://www.youtube.com/watch?v=zfw63uGGiDE.

[112] R. Fan, J. Dong, and A. Vishwanath, *Simulating the non-unitary Yang-Lee conformal field theory on the fuzzy sphere*, arXiv:2505.06342.

[113] J. E. Miro and O. Delouche, *Flowing from the Ising model on the fuzzy sphere to the 3D Lee-Yang CFT*, J. High Energy Phys. 10 (2025) 037.

[114] S. Mamone, G. Pileio, and M. H. Levitt, *Orientational sampling schemes based on four dimensional polytopes*, Symmetry **2**, 1423 (2010).

[115] M. Geck and G. Pfeiffer, *Characters of Finite Coxeter Groups and Iwahori-Hecke Algebras*, London Mathematical Society Monographs New Series (Oxford University Press, New York, 2000).